



Kaunas University of Technology

Faculty of Mechanical Engineering and Design

**Development of visible light spectrometer on the basis of
NIKON microscope for detection of bio-particle concentration**

Master's Final Degree Project

Harish Balasubramanian

Project author

Prof. dr. Giedrius Janušas

Supervisor

Kaunas, 2020



Kaunas University of Technology

Faculty of Mechanical Engineering and Design

Development of visible light spectrometer on the basis of NIKON microscope for detection of bio-particle concentration

Master's Final Degree Project

Mechanical Engineering (code 6211EX009)

Harish Balasubramanian

Project author

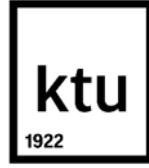
Prof. dr. Giedrius Janušas

Supervisor

Prof. habil. dr. Arvydas Palevičius

Reviewer

Kaunas, 2020



Kaunas University of Technology

Faculty of Mechanical Engineering and Design

Harish Balasubramanian

Development of visible light spectrometer on the basis of NIKON microscope for detection of bio-particle concentration

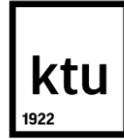
Declaration of Academic Integrity

I confirm that the final project of mine, Harish Balasubramanian, on the topic 'Development of visible light spectrometer on the basis of NIKON microscope for detection of bio-particle concentration' is written completely by myself; all the provided data and research results are correct and have been obtained honestly. None of the parts of this thesis have been plagiarised from any printed, Internet-based or otherwise recorded sources. All direct and indirect quotations from external resources are indicated in the list of references. No monetary funds (unless required by law) have been paid to anyone for any contribution to this project.

I fully and completely understand that any discovery of any manifestations/case/facts of dishonesty inevitably results in me incurring a penalty according to the procedure(s) effective at Kaunas University of Technology.

(name and surname filled in by hand)

(signature)



Kaunas University of Technology

Faculty of Mechanical Engineering and Design

Study programme: MECHANICAL ENGINEERING 6211EX009

Task Assignment for Final Degree Project of Master Studies

Student – Harish Balasubramanian

Title of the Project –

Development of visible light spectrometer on the basis of NIKON microscope for detection of bio-particle concentration

(In English)

Regimojo spektro šviesos spektrometro, pritaikyto Nikon mikroskopui ir skirto bio dalelių koncentracijos tyrimui, kūrimas

(In Lithuanian)

1. Aim and Tasks of the Project –

The aim of this thesis is to design visible light spectrometer for the NIKON microscope to detect bio-particle concentration. The following tasks are performed to achieve the goal,

1. To calculate the fluid flow in a microfluidic device.
2. To propose the concept of the visible light spectrometer and select the required components.
3. To fabricate a functional prototype of the designed visible light spectrometer.
4. To test the functionality of the developed visible light spectrometer.

2. Initial Data –

Nikon LV 150 microscope.

3. Main Requirements and Conditions –

Real-time optical – spectroscopy analysis when the sample is placed under the microscope.

Project author

Harish Balasubramanian

(Name Surname)

(signature)

(date)

Supervisor

Prof. dr. Giedrius Janušas

(Name Surname)

(signature)

(date)

Programme Director of the Study field

Assoc. prof. dr. Kęstutis Pilkauskas

(Name Surname)

(signature)

(date)

Balasubramanian, Harish. Development of visible light spectrometer on the basis of NIKON microscope for the detection of bio-particle concentration. Master's Final Degree Project/ supervisor Prof. dr. Giedrius Janušas; Faculty of Mechanical Engineering and Design, Kaunas University of Technology.

Study field and area (study field group): Technological Sciences, Mechanical Engineering,

Keywords: spectrometer, visible light, spectrum, wavelength

Kaunas, 2020. 55 p.

Summary

Techniques to analyse biological samples have been advancing rapidly in recent years. A biological sample has to be utilised up to a maximum extent, as it demands a lot of labour, capital, time and knowledge. The purpose of the project is to develop a visible light spectrometer in order to have two kinds of real-time analysis when the sample is placed under the microscope. A cost-effective visible light spectrometer is designed for the Nikon optical microscope. The fabricated spectrometer has been calibrated and tested using a periodic microfluid device and three fluids (water, glycerinum and olive oil). The resulting spectrum from the spectrometer is observed on the thermino spectrometer software, and the spectrums are compared with the spectrum found in the literature.

Balasubramanian, Harish. Regimojo spektro šviesos spektrometro, pritaikyto NIKON mikroskopui ir skirto bio-dalelių koncentracijos tyrimui, kūrimas Magistro baigiamasis projektas Prof. dr. Giedrius Janušas; Kauno technologijos universitetas, Mechanikos inžinerijos ir dizaino fakultetas.

Studijų kryptis ir sritis (studijų krypčių grupė): Mechanikos inžinerija, Technologijos mokslai.

Reikšminiai žodžiai: spektrometras, matoma šviesa, spektras, bangos ilgis

Kaunas, 2020. 55 p.

Santrauka

Pastaraisiais metais sparčiai tobulėja biologinių mėginių analizės metodai. Biologinių mėginių analizei reikia daug darbo, kapitalo, laiko ir žinių. Magistrinio darbo tikslas yra sukurti matomos šviesos spektrometrą, kad būtų galima atlikti dviejų rūšių realaus laiko analizę, kai mėginys tiriamas po mikroskopu. Darbe pristatomas sukurtas ekonomiškasis matomos šviesos spektrometras, kuris bus suderinamas su Nikon optiniu mikroskopu. Pagamintas spektrometras sukalibruotas ir ištirtas naudojant periodinį mikroskystinį prietaisą ir tris skysčius (vanduo, glicerinas, alyvuogių aliejus). Gauti bandinių spektrai užregistruoti programa Thermino Spectrometer ir palyginti su literatūroje randamais spektrais.

Table of Contents

List of figures	8
List of tables	10
Introduction	11
1. Literature review	12
1.1. Mass spectrometer	14
2. Visible light spectrometer	20
2.1. Thermino software.....	21
3. Analysis of microstructure.....	24
4. Construction of spectrometer	31
4.1. Manufacturing of the spectrometer parts.....	33
4.2. Selection of camera	34
4.3. Selection of dispersing element.....	35
4.4. Final assembly of the spectrometer	37
5. Experimental setup.....	41
6. Results and discussion	45
6.1. Olive oil spectrum	47
6.2. Glycerinum spectrum	49
6.3. Water spectrum:.....	50
Conclusions	52
References.....	53
Appendices	56

List of figures

Fig. 1 Electromagnetic spectrum [1]	12
Fig. 2 Energy level diagram for the absorption and emission [1]	13
Fig. 3 a) The schematic of overall working of mass spectrometer [3]; b) Working of electron ionisation source [3]	14
Fig. 4 Different types of mass analyser a) Quadrupole mass analyser [4]; b) Time of Flight mass analyser [4]; c) Ion trap analyser [4]; d) Magnetic sector mass analyser [4]; e) Electrostatic sector mass analyser [4]; f) Combined electric and magnetic mass analyser for double-focusing [3]	15
Fig. 5 Fabry Perot sensor with integrated micro/nanofluidic channels [11].....	17
Fig. 6 Working of surface plasmon imaging [13]	18
Fig. 7 Localised surface plasmon resonance imaging in a) transmission mode and b) reflection mode [14]	18
Fig. 8 a) Working of the single beam spectrometer, b) working of the double beam spectrometer [16]	20
Fig. 9 a) Working of photodiode array spectrometer [16]; b) Flow of microscopic light from the microscope through the sample and spectrometer.....	21
Fig. 10 Fullscreen view of thermino software.....	22
Fig. 11 Upper and lower command bar	22
Fig. 12 a) Video control panel; b) Input panel	23
Fig. 13 a) Save image dialogue box; b) Available image formats; c) Video input device panel which shows the information about the used camera.....	23
Fig. 14 Microstructure dimensions.....	24
Fig. 15 a) Model builder window; b) Block 1 dimension; c) Block 2 dimension; d) Block 3 dimension.	26
Fig. 16 a) Created geometry; b) Block 2 geometry is selected for laminar flow analysis.	27
Fig. 17 a) laminar flow selection; b) Fluid properties selection; c) inlet selection; d) outlet selection.	28
Fig. 18 a) Meshing of the laminar flow surface b) Transparent view of the mesh throughout the microchannel c) Mesh view.....	28
Fig. 19 Reynolds number vs Velocity	30
Fig. 20 Nikon LV 150 microscope	31
Fig. 21 Stage movement knob and focus knob for focusing the image	32
Fig. 22 The main assembly box.....	33
Fig. 23 Top cover for the spectrometer	34
Fig. 24 Side cover for the spectrometer.....	34
Fig. 25 a) Trust web camera used in the spectrometer; b) Removal of IR filter	35
Fig. 26 a) prism; b) Diffraction grating used in the spectrometer	36
Fig. 27 a) Transmission mode of the grating; b) Reflection mode; c) Both reflection and transmission mode in the grating	36
Fig. 28 Black paint given to the manufactured parts.....	37
Fig. 29 a) Position of the camera ;b) Position of the mirror.....	38
Fig. 30 Flow of light inside the spectrometer	39
Fig. 31 Full view inside the spectrometer.	39
Fig. 32 Assembled visible light spectrometer	40

Fig. 33 Microfluidic channel network	41
Fig. 34 The green laser and red laser used for calibration.....	41
Fig. 35 The path to select trim points	42
Fig. 36 Spectrum of the green laser without the calibration.....	43
Fig. 37 The spectrum of green laser with a peak at 528 nm obtained after calibration.....	43
Fig. 38 The spectrum of red laser with a peak at 632 nm	43
Fig. 39 The entire experimental setup	44
Fig. 40 Spectrum of the microscope light (halogen lamp)	45
Fig. 41 Spectrum of the polycarbonate material.....	46
Fig. 42 a) Microscopic image of polycarbonate; b) Microscopic image of the microfluidic channel network	46
Fig. 43 Spectrum of the microfluidic channel network.	47
Fig. 44 Absorbance caused by the period of the microstructure [24].....	47
Fig. 45 a) Absorbance spectrum of olive by Dr.Cosimo et al. [25]; b) Microscopic image of olive oil	48
Fig. 46 Spectrum of the olive oil	48
Fig. 47 Spectrum of the glycerinum obtained from the spectrometer	49
Fig. 48 a) Absorbance of glycerol spectrum [26]; b) Microscopic image of glycerinum	49
Fig. 49 Spectrum of water on the microfluidic channel network.	50
Fig. 50 a) The water absorption spectrum over the entire electromagnetic radiation [27]; b) The microscopic image of the water on the microfluidic channel network.....	51

List of tables

Table . 1 Sources of radiation for spectroscopy and its corresponding technique [1].....	13
Table . 2 Properties of the sample [19] [20]	25
Table . 3 Reynolds number for three sample specimen.....	26
Table . 4 Results of simulation	29
Table . 5 Maximum velocity obtain from simulation and corresponding Reynolds number.....	30
Table . 6 Deflection in degrees	38

Introduction

The biological system covers a vast range of particles whose size span from metre to picometre. A biological system comprises of both macromolecule and micromolecule, which is responsible for the effective functioning of that living system. Therefore, understanding the behaviour of the biological systems is necessary for the in-depth research and development of the systems. To understand the functioning of the living systems, it is essential to know the characteristics of each molecule that are contributing to the system. The research on the characterisation of these molecules has been performed from the early scientific age, and whenever a particular question is answered, which leads to a new question about the living system. To know the characteristics of a molecule in a biological system, it is essential to detect the presence of that molecule in the system. From a wide range of detection techniques, optical detection technique is most important for the detection of a molecule using the light as a source of detection. In a vast world where different kinds of biological systems exists, it is difficult to analyse the microscopic properties of living organisms with mere vision of the naked eyes to an extent, characteristics of those organisms that are on a macroscopic scale such as colour, shape, texture etc., can be determined with the human eye. However, when there is a need for understanding the properties on a microscopic scale, the necessity for usage of technical equipment emerge. Out of many techniques which are based upon electrical, chemical and physical methods, optical detection technique is taken as the subject of interest. Various optical detection techniques have been developed over the years and in which spectroscopy is a significant detection technique. Spectrometer studies the interaction of light with the compound of interest. With a particular spectrometer, only a particular biological question can be answered due to the physical limits on the spectrometer. The usefulness of a spectrometer is, therefore, a trade-off between its purpose and the employed spectroscopic method. The cost of the spectrometer is also an essential factor for selecting a spectrometer. A high-resolution Ocean optics spectrometer would cost a few thousand euros, which may not be affordable for a few research purposes.

The aim of this thesis is to design visible light spectrometer for the NIKON microscope to detect bio-particle concentration. To achieve the aim, the following tasks are performed.

1. To calculate the fluid flow in a microfluidic device.
2. To propose the concept of a visible light spectrometer and select the required components.
3. To fabricate a functional prototype of the visible light spectrometer.
4. To test the functionality of the developed visible light spectrometer.

1. Literature review

Optical spectroscopy is the method which utilises optical materials to disperse the light and focus them. The optical spectroscopy covers the spectrum that is observed in the ultraviolet, visible and infrared region. The term spectroscopy refers to the optical spectroscopy or photon spectroscopy since optical elements have a major role in obtaining the spectrum. Electromagnetic radiations consist of radio waves, infrared, visible light, microwaves, ultraviolet, X-rays and gamma rays. Electromagnetic radiation is a form of energy which explains the dual nature of light (i.e.) light as particle and wave. The particle nature of light is explained by the optical properties such as transmission whereas, the other optical properties such as absorption and emission describes the wave nature of light. Each type of radiations is emitted as a result of the interaction of light with the matter. As a result of the interaction, radiations are emitted, which forms the electromagnetic spectrum of light which are created due to various atomic transitions. Figure 1 shows the electromagnetic spectrum due to the molecular or atomic transitions.

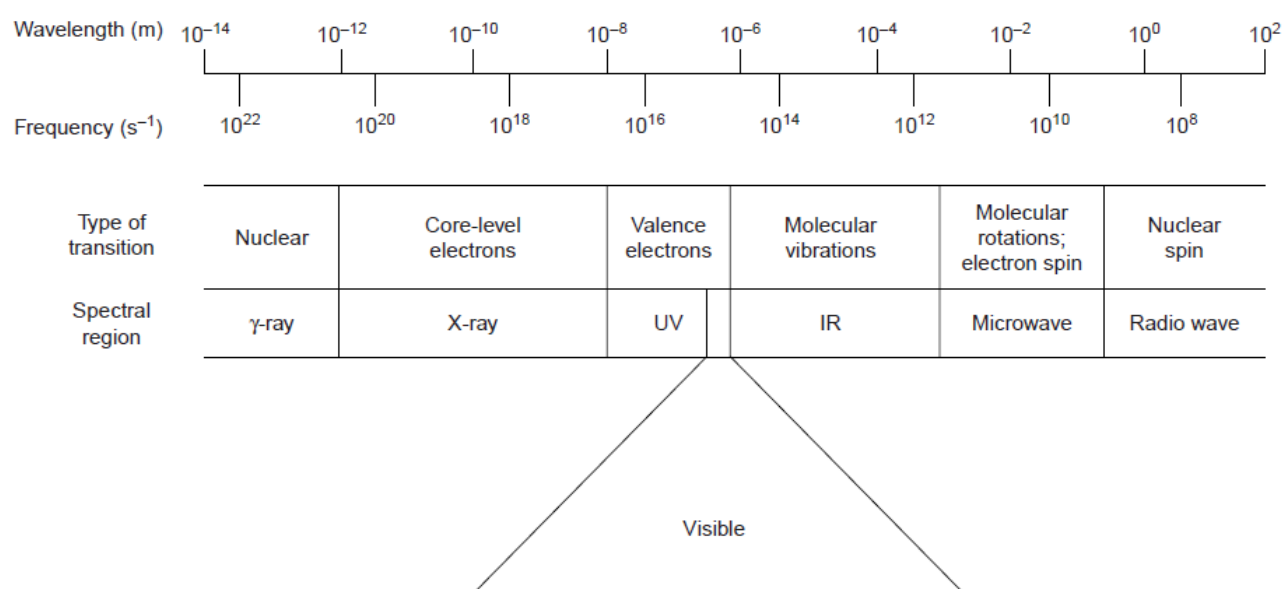


Fig. 1 Electromagnetic spectrum [1]

In the electromagnetic spectrum, the boundaries formed by each type of radiation is not rigid, which leads to the overlapping of spectral lines [1]. The interaction of a photon with the sample is crucial for spectroscopy. The spectroscopic techniques are broadly classified into two types. In the first type, the energy of the photon is absorbed by the atoms. This absorption causes the atom to excite from a lower energy level to a higher energy level. The spectrum obtained as a result of this energy transition is known as the absorption spectrum. The absorption spectrum in the UV visible region is measured by the energy of valence electron in higher energy state after excitation. However, the type of measurement of radiation after absorption is highly dependent on the type of radiation. In case of infrared radiation, the chemical bonds experience the change in vibrational energy which can be detected using infrared spectroscopy. The absorption of the photon is only possible when the difference between the two energy levels is equal to the energy of the photon. The absorbance of an analyte is usually measured with the percentage of transmittance, and it varies from 0% (full absorption) to 100% (no absorption). If the absorbance is low, then the sample has high transmittance. The second type of measurement is known as Emission. The interaction of light with the analyte causes a transition of the atom from a higher energy level to a lower energy level by emitting a photon

which is equal to the difference in energy between the two energy levels. The higher energy level of the electrons in the analyte is achieved by thermal energy, chemical energy (or) radiation by a photon. Figure 2 shows the energy differences during atomic or molecular transitions caused by the absorption spectrum and emission spectrum. Table 1 shows the type of radiation for both absorption and emission and its corresponding spectroscopic technique.

Table . 1 Sources of radiation for spectroscopy and its corresponding technique [1]

Type of energy transfer	Region of the Electromagnetic spectrum	Spectroscopic technique
Absorption	γ - ray	Mossbauer spectroscopy
	X-ray	X-ray absorption Spectroscopy
	UV/vis	UV/Vis spectroscopy Atomic absorption spectroscopy
	Infrared	Infrared spectroscopy Raman spectroscopy
	Microwave	Microwave spectroscopy Electron spin resonance spectroscopy
	Radio waves	Nuclear magnetic resonance spectroscopy
Emission	UV/Vis	Atomic emission spectroscopy
	X-ray	X-ray Fluorescence
	UV/Vis	Fluorescence spectroscopy Phosphorescence spectroscopy Atomic fluorescence spectroscopy

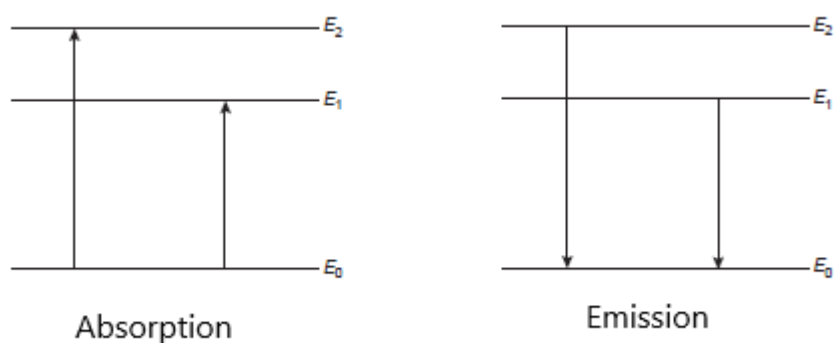


Fig. 2 Energy level diagram for the absorption and emission [1]

The basic operation of the spectrometer is to focus the light passed through the dispersing element and passing it through the sample. Therefore the necessary components are a light source, a detector element, a dispersing element and a focusing element based upon the requirement. The source of light plays a vital role in determining the output of the spectrometer. The light source must be intense and able to produce a different spectrum when the sample is tested. Also, each light source has its applications depending upon the wavelength that should be detected. A continuum source emits

radiation over a wide range of wavelength, and a line source emits light at a particular wavelength. For the absorption spectrum, energy from photon is sufficient to produce a spectrum, whereas the emission spectroscopy requires thermal or chemical energy to produce a spectrum. Next, the selection of detector elements plays an important role in the output spectrum. Human eyes were used as a detector in the early age, eg. In Nessler's colourimetric method [1]. Modern spectrometers use transducers which converts a photon into an electrical signal such as current or voltage. Most commonly used transducers for spectrometer are classified into two types, i) Photon transducers ii) Thermal transducers. Photon transducers have a photosensitive surface which produces an electrical signal by absorbing photons when the light is incident on its surface. The light measurements can be from ultraviolet, visible or near infrared region. However, at the infrared and far-infrared region, the detection using photon transducers are difficult. Hence, thermal transducers are employed in case of infrared spectroscopy. In thermal transducers, the energy of photon causes an increase in temperature, which is converted into an electrically measurable signal such as current and voltage.

1.1. Mass spectrometer

Mass spectroscopy is an analytical method in which a mixture of substance is separated in to beam of particles which are crooked by an electric and magnetic field to produce a spectrum which differs according to the type of atom present in the beam [2]. The analytes in the mass spectrometer are detected by measuring the mass to charge ratio [3]. The working of the mass spectrometer is shown in figure 3a. The mass spectrometer is classified depending upon the ionisation source and type of mass analyser. The two major ionisation sources in a mass spectrometer are i) Chemical ionisation and ii) Electron ionisation.

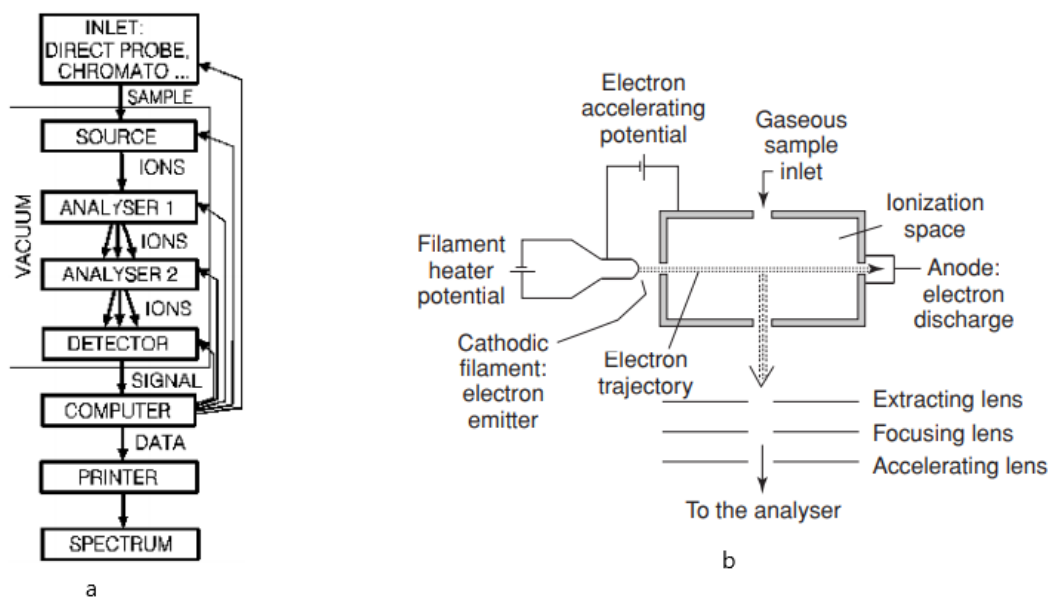


Fig. 3 a) The schematic of overall working of mass spectrometer [3]; b) Working of electron ionisation source [3]

Electron ionisation or electron impact consist of heated filament which gives electrons and directed to the anode trap. The sample analyte collides with the electron beam, which leads to the formation of analyte molecular ions. The schematic representation of the working of electron ionisation is shown in figure 3b. Electron ionisation leads to the formation of fragmentation of the molecular ion. The

presence of molecular ion prevents the detection of the molecular weight of the ion. Alternatively, chemical ionisation produces ion with little excess energy and less fragmentation. Chemical ionisation produces fragmentation of ions by colliding the molecule to be analysed with the primary ions in the source. The advantage of chemical ionisation is that it produces less fragmentation and hence the molecular weight information can be obtained as the output, which is not possible in the case of electron ionisation.

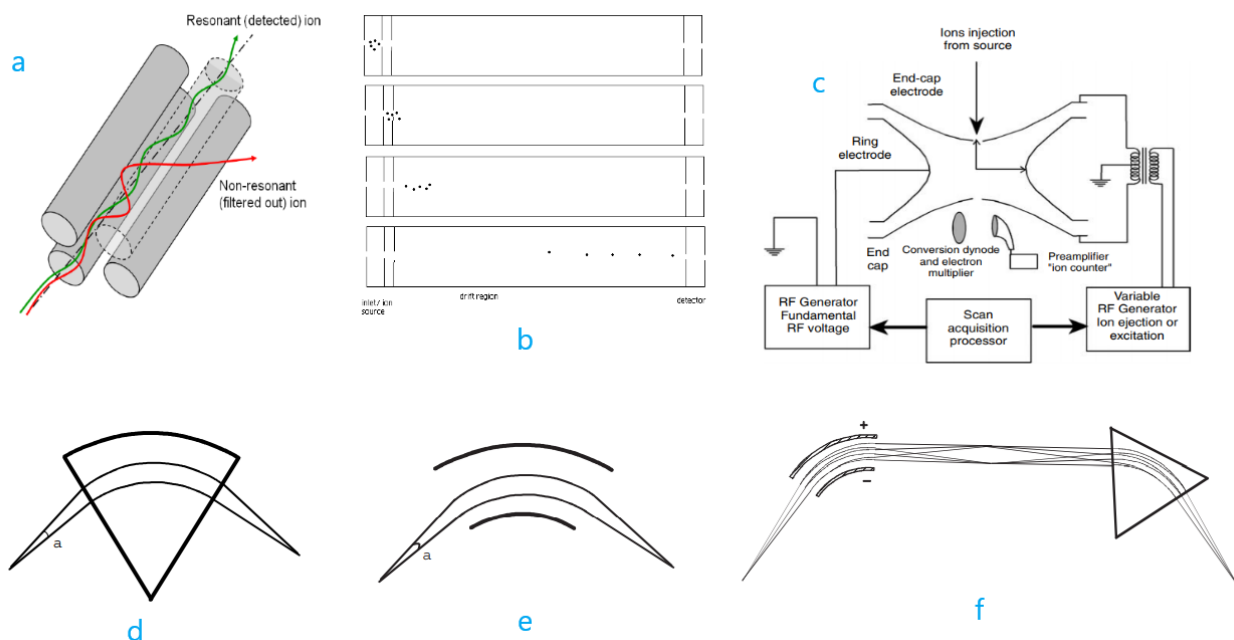


Fig. 4 Different types of mass analyser a) Quadrupole mass analyser [4]; b) Time of Flight mass analyser [4]; c) Ion trap analyser [4]; d) Magnetic sector mass analyser [4]; e) Electrostatic sector mass analyser [4]; f) Combined electric and magnetic mass analyser for double-focusing [3]

The electrons from the source is passed through the analyser and reaches the detector. The different types of mass analyser are i) Quadrupole mass analyser, ii) Time of flight mass analyser, iii) Ion trap analyser, iv) Electrostatic mass analyser, v) Magnetic mass analyser. The variation in the mass analysers is due to the variation in the separation technique of ion that hits the detector [5]. In quadrupole mass analyser, the ionised analyte enters the oscillating electric field created by four circular electrodes, as shown in figure 4a. By varying the potentials of the electrode, the charged particle will be accelerated in a spiral path and reach the detector. In quadrupoles, the particle with specific mass to charge (m/z) ratio travels in a spiral path while the ions with different m/z ratio are absorbed by the electrodes. The ion trap analyser was first described by Paul & Steinwed as “ion trap”. The working of the ion trap analyser is shown in figure 4c. The charged ions are trapped inside the four electrodes and are ejected from the trap according to their masses which reaches the detector, to obtain the spectrum [3]. In Time of Flight (TOF) mass analyser (shown in figure 4b), the charged ions after initial acceleration enter into a flight tube where ions are separated based upon the velocity of the charged ions [1]. TOF mass analyser has a limitation for ions with higher masses since it takes a longer time to reach the detector, and hence its resolution is limited [4]. The electrostatic mass analyser consists of two curved plates of equal and opposite potential and the entire setup is shown in figure 4e. The working of the electrostatic mass analyser is similar to Time of Flight mass analyser, except electric field is used in the electrostatic mass analyser. When the ions travel through the electric field, it is deflected by an energy and this energy is equal to the centripetal force of the ion [4]. Hence

the kinetic energy will be available with the ion, and this energy is used by the ions to reach the detector, and the remaining ions are dispersed. The magnetic mass analyser uses the momentum of the ions to reach the detector. The working of the magnetic mass analyser is similar to the electrostatic mass analyser except the magnetic field is used to produce deflection instead of the electric field and is shown in figure 4d. The schematic diagram of the electrostatic and magnetic mass analysers combined are shown in figure 4f. The combination of electric and magnetic mass analysers can create double-focusing. The mass spectrometer can be integrated with the chromatography techniques, which leads to the formation of an instrument with both separation and detection. The most commonly used instruments are Liquid Chromatography-Mass spectrometer [LC-MS] [5] and Gas Chromatography-Mass spectrometer [GC-MS] [5]. The results from LC-MS and GC-MS are more accurate and are used in industries for detecting the adulterations present in the sample and for determining the particles present in the analyte. These instruments are expensive, and hence its applications are limited.

Apart from spectroscopy, researches are being conducted, focusing on the usage of optofluidics for detection techniques. The term 'Optofluidics' was first discovered in 2003, by Defense Advanced Research Project Agency (DARPA) and the motive was "to develop adaptive optical circuits by integrating optical and fluidic devices" [6]. The development in the field of microfluidics in recent years shows a sharp increase and this gave way for the development for a new type of fluid known as optofluidics. It is well suited for biological and chemical detection in small volumes (μl to nL) because of its customised properties [7]. Optical properties such as refractive index, scattering, absorption and polarisation can be integrated with the microfluids for bio/chemical analysis [7]. The fluid-fluid interaction techniques can be used to change the optical properties of the device by changing the fluid in the medium. The presence of surface tension between the fluids is advantageous, and different layers can be formed in the optofluidic chip. With droplet of fluid between two immiscible liquid can be used as a lens which can be tuned to concave and convex mode based upon the requirement [8]. The fluid can be used to manipulate micro and nano-size objects, and this is known as optical tweezers [9]. The optical force can be employed on a fluid which can be used as a transport medium for the transport of molecules. It is well suited for biological and chemical detection in small volumes because of its customised properties [6]. It creates a path by using optofluidic devices with detector elements for optical detection of biological samples, and optical biosensors are based on this principle. A brief description of the operating principle, classification and the bioanalytical applications of an optical biosensor are explained here. Optical biosensors allow for selective and sensitive detection of wide range analyte including virus, drugs, antibodies and tumour cells. The main advantage of using optical biosensor is that they provide direct, real-time and lab free detection of many biological and chemical substances. Over other sensing techniques, research and development of optical bio-sensor have increased, and they find various applications in streams such as microelectronics, MEMS, micro/nanotechnologies, molecular biology, biotechnology and chemistry [10]. Optical biosensor work by exploiting the interaction between the optical field and bio-recognition element. They can be further divided into label-free and label-based methods. In the label-free method, the interaction between the bio-particle takes place without any external force, and the output is recorded as an electrical signal using a transducer. In case of label-based mode, the bio-particle interaction is stimulated with the use of external forces such as fluorescence (or) luminescence to generate the signal. However, in some cases, labelling can alter the binding properties of the interacting bio-particle resulting in a systematic error. The optical biosensor is a compact analytical device which can produce a signal proportional to the concentration of the

measured substance which includes various biological materials. There are many applications based on this type of optical detection technique, out of which some of them are discussed below,

Optofluidic sensors based on Refractive Index (RI) uses refractive index property for detection in bio/chemical analytical methods. It is categorised as a label-free sensing technique. The sensors measure/detect the refractive index changes in the sample solution to produce results. They are best suitable for low detection volumes. Some of the commonly used architectures are photonic crystals (PC), photonic crystal fibres (PCF), Mach-Zender interferometers, ring resonators, Fabry Perot cavities. A Fabry Perot sensor is shown in figure 5. PC and PCF based optofluidic refractive index (OFRI) sensors primarily employ periodic structures to continue and guide the light [7]. The optofluidic ring resonator architecture uses thin-walled cylindrical capillaries, self-assembled tables on-chip, glass microbubbles and antiresonant reflecting optical waveguides (ARROW), equipping them with excellent sensing capability while also forming integrated microfluidic structure [7]. The mass transport of the target molecules to the sensor surface is one of the common problems faced by the photonic sensors. This problem is encountered by using optofluidic flow-through strategy. This technique integrates microfluidic channels through the optical sensing structures so that the entire sample reacts with the sensitive surface. OFRI sensors can be incorporated with conventional analytical chemistry techniques such as chromatography to enhance biosensing capabilities.

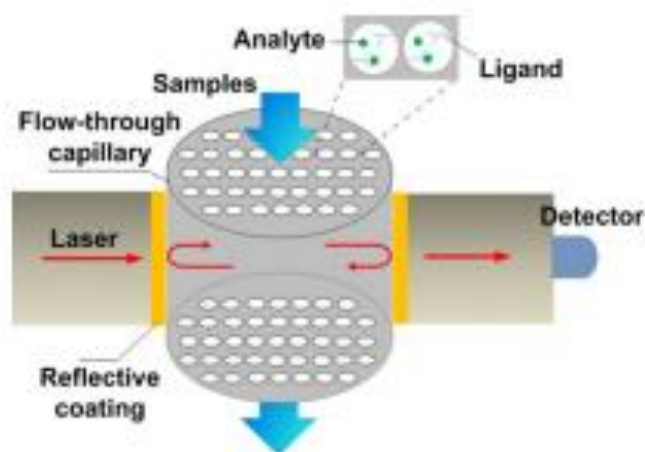


Fig. 5 Fabry Perot sensor with integrated micro/nanofluidic channels [11]

Surface Plasmon Resonance (SPR) based biosensor is a widely used type of optical biosensing method. Surface plasmon resonance occurs on the surface of the metal, i.e., plasmons are generated on the surface at the intersection of two medium (commonly glass and liquid) when it is illuminated by the polarised light at a particular angle. This phenomenon is proportional to the mass of the surface. SPR based biosensing is a direct, label-free method. It can detect real-time changes of the refractive index at the sensor surface, which is proportional to the biomolecule concentration. A sensogram can be obtained by measuring the shift of reflectivity, angles or wavelength against time. An SPR instrument is shown in figure 6, which consists of an optical detector to measure the intensity shift, a gold-coated sensor and a layer to enable the liquid immobilisation. This layer is integrated with the fluidics system to enable flow-through operation. Surface plasmon resonance imaging is an extension of SPR analysis. It is the combination of spatial imaging in the microarray and the sensitivity of SPR, which allows for simultaneous study of different interactions [12]. Surface plasmon resonance imaging has a great future because of its high throughput sensitivity and ability to resolve images of biological interactions spatially.

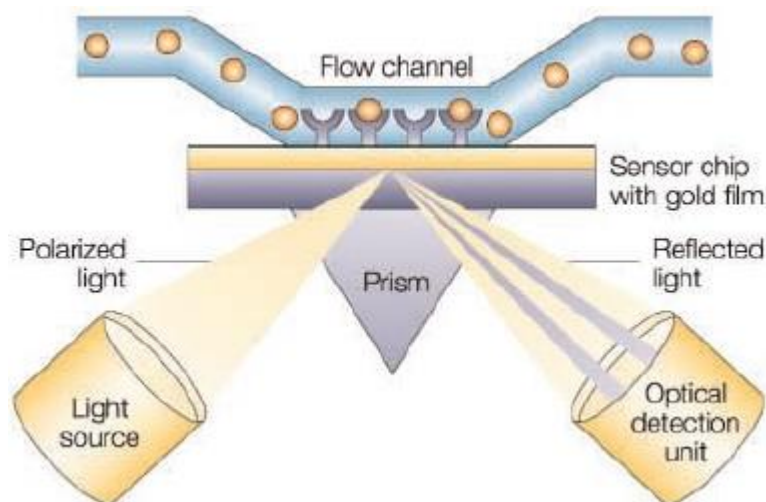


Fig. 6 Working of surface plasmon imaging [13]

Localised Surface Plasmon Resonance imaging (LSPRi) is based on metallic nanostructures. These metallic nanostructures have unique optical properties which are not seen in the large metal structures. When the light is incident on the metallic nanostructures, electron charge oscillations are induced on the surface of the metallic nanostructures. Due to this oscillation, the absorption of light takes place. This absorption corresponds to the wavelength of light in the UV-Visible region. This is the principle behind localised surface plasmon resonance. In LSPRi, the induced plasmons oscillate locally on the metallic nanostructures rather than the metal/dielectric interface. It differentiates the localised surface plasmon resonance from surface plasmon resonance [7]. Figure 7 shows a localised surface plasmon biosensor with transmission mode and reflection mode used for the detection of molecules [14]. The efficiency of LSPRi is largely dependent on factors such as size, the material used, interparticle distance and shape of the metallic nanostructure, which are expressed as a change in colour and peak absorption. By manipulating the parameters mentioned above, the LSPR sensor properties can be controlled/optimised. Detection based on LSPRi is easier to miniaturise, to improve detection throughput and reduce the operating costs.

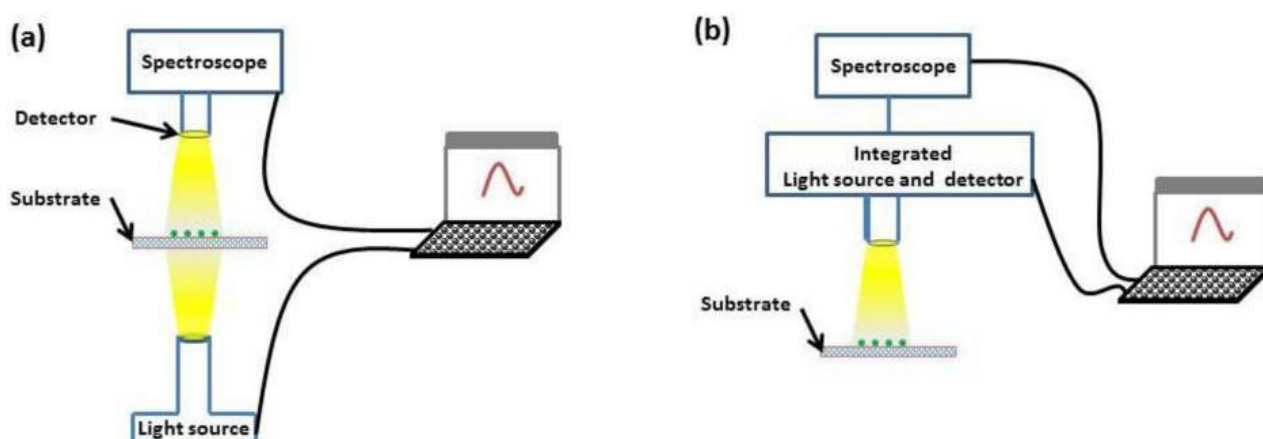


Fig. 7 Localised surface plasmon resonance imaging in a) transmission mode and b) reflection mode [14]

Surface Enhanced Raman Spectroscopy (SERS) may have the potential of being a label-free technique which has low detection limits compared to fluorescence-based spectroscopy, while also

providing molecule-specific Raman spectrum for analyte identification. SERS exploits the well-understood electromagnetic enhancement produced by metal nanostructures, as well as chemical enhancement due to interactions between metal and molecule, which is not yet fully explored. Even though SERS has been on research for more than 35 years [15], the practical application of this technique is still limited. As mentioned above, the mechanisms responsible for SERS process is divided into two i) Electromagnetic ii) Chemical. In electromagnetic, the interaction of the light with metal leads to the induction of enhanced electromagnetic fields. The resonance of the surface plasmons intensifies the electric field upon interaction with the photon of the incident light. The metallic properties of the surface influence the plasmon resonance frequency [15]. The interaction between the plasmons of a colloidal metal structure with incident light upon the analyte molecules is responsible for the electromagnetic SERS enhancement [15]. In the chemical mechanism, the charge-transfer complex between analyte molecule and the surface, an electromagnetic field is induced. The induced electromagnetic field amplifies the molecular electronic state by molecular interaction with the metal surface. The practical use of SERS can be increased by integrating the functions. The typical implementation include i) metal nanoparticle colloidal solution is used to pass the sample through the channel, ii) metal nanostructural surface is integrated to the bottom of the microfluidic channel. SERS measurement in a microfluidic environment has detection limits due to the low number of SERS active sites. By increasing the number of target analyte molecules to the SERS active surface, high transport of analyte molecules can be attained. This increases the efficiency of Surface Enhanced Raman Spectroscopy. The applications of SERS will continue to expand from new advancements in optofluidics such as the introduction of optically active resonant microstructures, integration of SERS with droplet microfluidics and optical trapping of nano-sized particles [15].

2. Visible light spectrometer

The purpose of this project is to develop a visible light spectrometer, and hence the explanation is limited to the UV visible light spectroscopy. The visible light has a wavelength range of 380 nm to 740 nm. Nessler's colourimeter method for determination of the concentration of ammonia forms the basis of the visible light spectrometer in which the human eye is used as a detector since human eyes can observe light only in the visible range [1]. The different types of visible light spectrometer are single beam spectrometer and double beam spectrometer. The single beam spectrometer as the name suggests applies a single beam onto the specimen. The light from the source is first passed through a monochromator and then through the sample specimen and then reaches the detector. A light of particular wavelength is only emitted on the sample to be tested, and this particular wavelength of light can be altered based upon the requirement. The working of the single beam spectrometer is shown in figure 8a. The blank is tested first with the spectrometer and is followed by the specimen. The spectral difference between the sample spectrum and blank spectrum gives information about the concentration of the particle in the sample specimen. The double beam spectrometer uses two separate beams for the sample and blank from a monochromator using mirrors. The working of the double beam spectrometer is shown in figure 8b. The light from the source is passed through a monochromator in which a light of a particular wavelength is split into two beams which passes through the sample and blank and then reaches the detector. A chopper controls the path of radiation between the sample and the blank specimen.

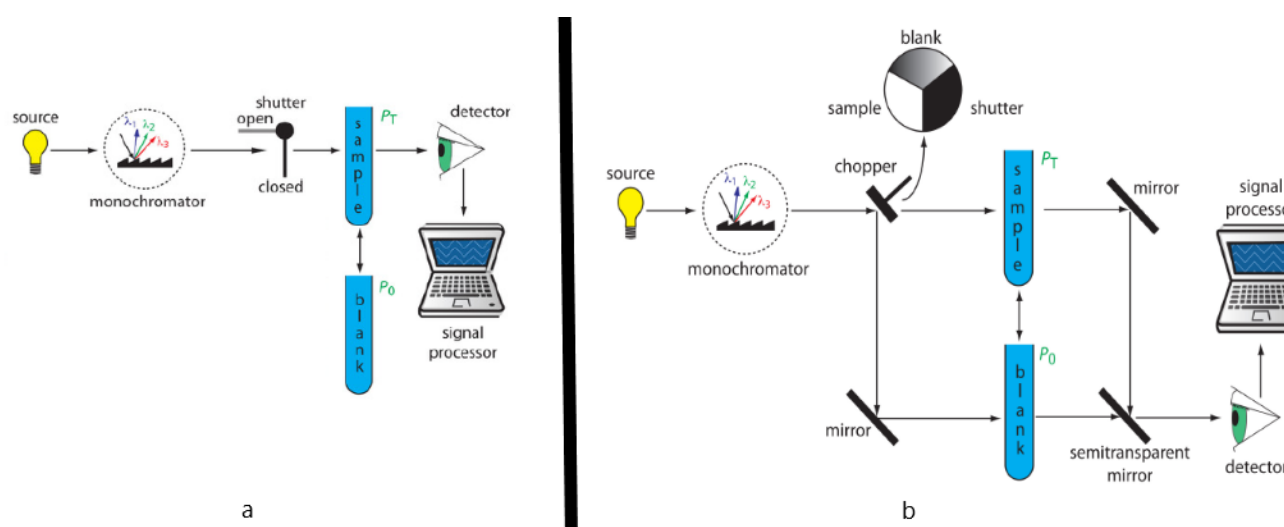


Fig. 8 a) Working of the single beam spectrometer, b) working of the double beam spectrometer [16]

Another type of spectrometer known as diode array spectrometer in which the light from the source is passed through the sample and then reaches the grating. The light from the grating is dispersed into different colours (VIBGYOR*) and then observed on the detector. The detector used is an array of photodiode which acquires data to form the spectrum of the light. A simple diode array spectrometer is shown in figure 9a.

*VIBGYOR refers to colours in visible light. The colours are Violet, Indigo, Blue, Green, Yellow, Orange and Yellow.

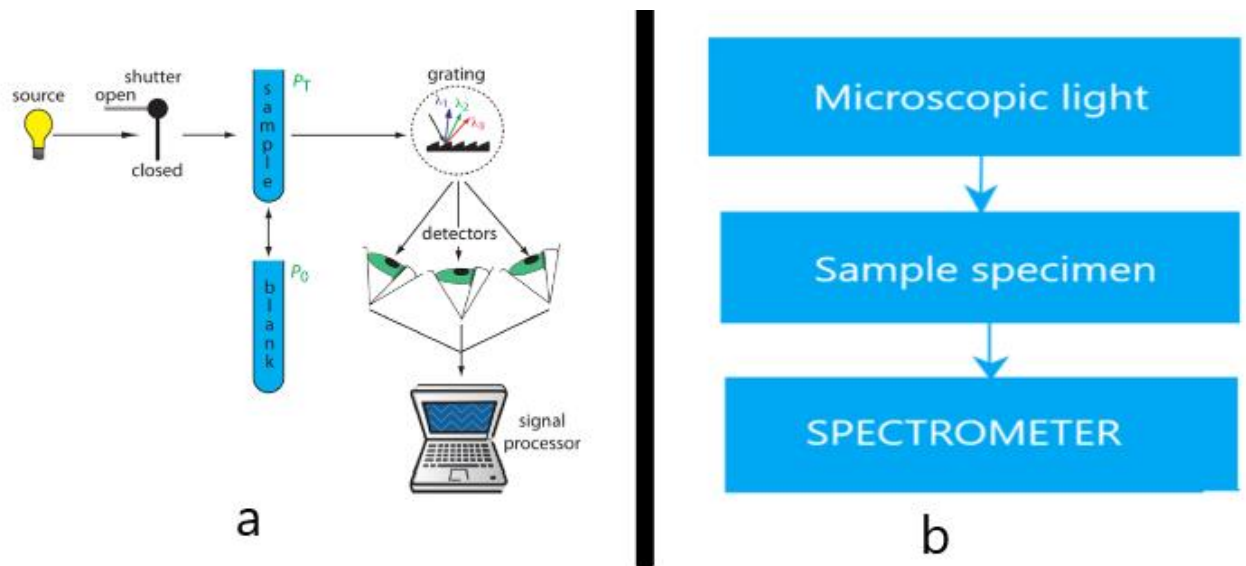


Fig. 9 a) Working of photodiode array spectrometer [16]; b) Flow of microscopic light from the microscope through the sample and spectrometer.

When a sample is placed under a microscope, the characteristics of the sample can be analysed. In case of biological samples, it has to undergo different kinds of processes such as air drying, chemical fixation followed by the critical point drying/ freeze fixation followed by critical point drying etc., in order to be observed under the microscope. This whole process of preparation of the sample can be highly time-consuming. After the preparation of the biological sample, it has to be placed on the microfluidic channel network for the examination of the specimen under the microscope. Moreover, while the sample is being examined, it has to be utilised in the most efficient way possible. With the help of the microscope, the size, shape and arrangement of the particle present in the sample. Apart from these observations, spectroscopy can offer the necessary tools to investigate the relevant structure and function of the sample. A spectrum of the sample can be obtained by integrating the spectrometer into the microscope. The spectrometer uses the light from the microscope as the source of the light, which reaches the spectrometer through the sample specimen. Thus, the spectrum of the sample specimen is obtained when the specimen is under microscopic observation. When considering the microscopic and spectroscopic results, more information about the properties of the particles or sometimes detection of new types of particles may be known. It paves the way for the two types of real-time analysis when the sample is placed under the microscope. A schematic representation of the analysis of the sample with the microscope and spectrometer are shown in figure 9b. In this project, a spectrometer is designed and developed for a NIKON LV150 microscope, and the resulting spectrum are observed in the thermino software. The spectrometer to be designed is based on the photodiode array spectrometer.

2.1. Thermino software

Thermino software is used to obtain the spectrum from the web camera. The thermino software is a stand-alone software and is available for free to download. This software is selected to use with the designed spectrometer, because of its accuracy and free availability, thus saving the cost as well as with no compromise in accuracy. The software main screen is shown in figure 10. The main screen has a separate column for slit image and spectrum image. The camera input can be controlled in a video input control box.

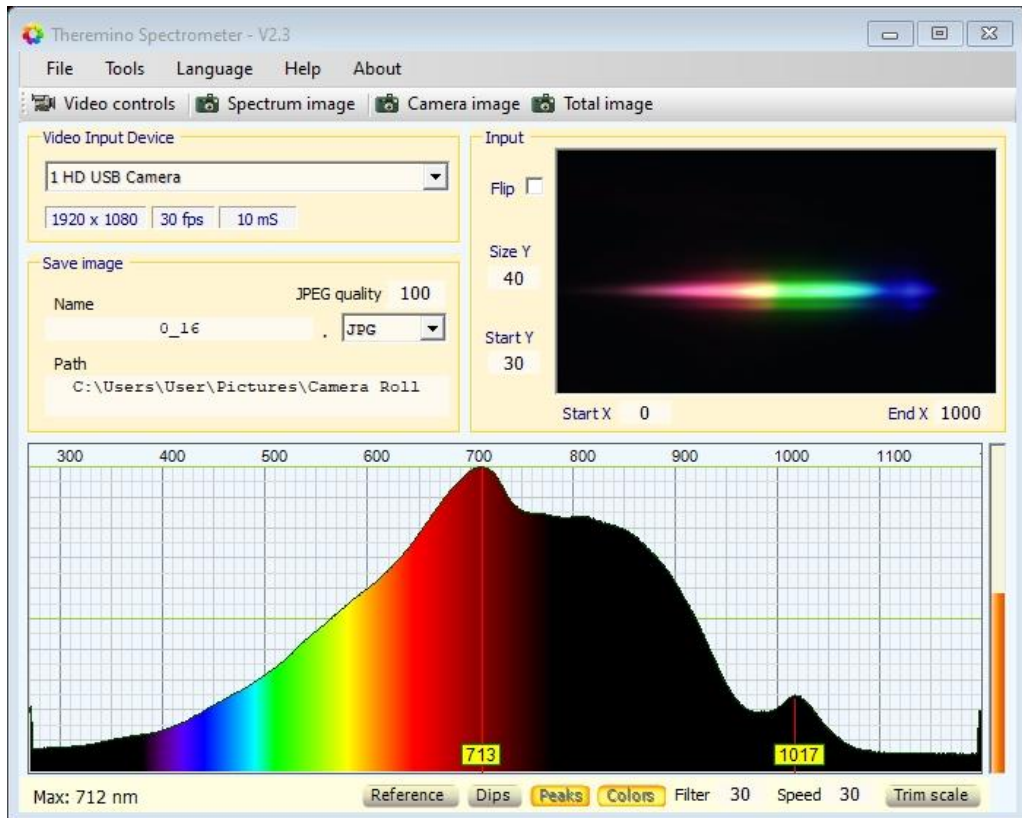


Fig. 10 Fullscreen view of theremino software.

The upper command bar is shown in figure 11, which has the provision for storing the different versions of the image. The total image is used to save the entire main screen. The camera image is pressed to save only the image obtained from the camera. The spectrum image is selected to save only the spectrum image. The lower command bar (shown in figure 11) is used for altering the spectrum image based upon the requirement. Dips command enables labels for minimum graph measurement. Peaks command labels the values of peak points on the graph. The colours command displays the colours of the corresponding wavelength in the image of the spectrum.

UPPER COMMAND BAR



LOWER COMMAND BAR

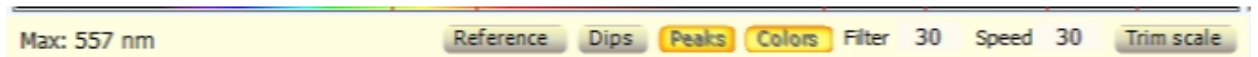


Fig. 11 Upper and lower command bar

The input panel contains the image of the camera and is shown in figure 12 b. The flip command is used to flip the image if the orientation of the image is not the same, as shown in figure 12 b. The X-axis and Y-axis values are altered to centre the spectrum within the orange box. Frequently, the software determines the position of the slits correctly. Usually, the Y-axis is changed to reduce the upper and lower limits to centre the image within the orange box.

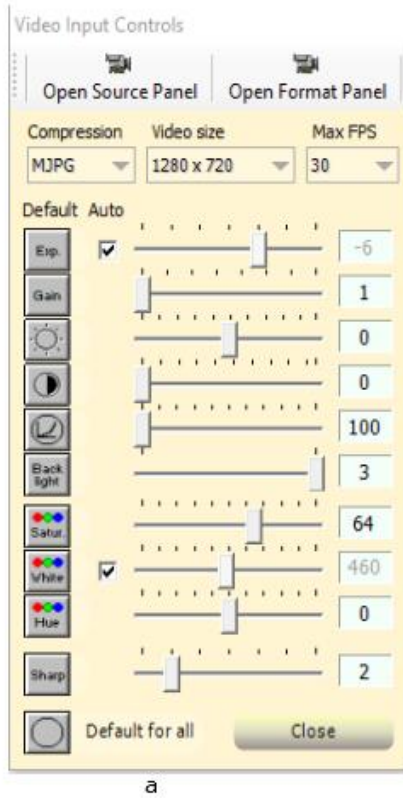


Fig. 12 a) Video control panel; b) Input panel

The video controls options dialogue box displayed adjacent to the main screen has controls to change the image parameters based upon the requirement (shown in figure 12 a). These settings have to be entered while opening the software every time since it cannot be stored. Usually, with the default settings, the image obtained in the software is good.

The video input device panel gives details about the camera used and its resolution. It is shown in figure 13 c. The first column tells about the resolution of the camera used. The **11 mS** indicates the time take (in milliseconds) by the software to process the image. The **6 fps** box shows the frames per second. This usually maintained from 6 fps to 9 fps.

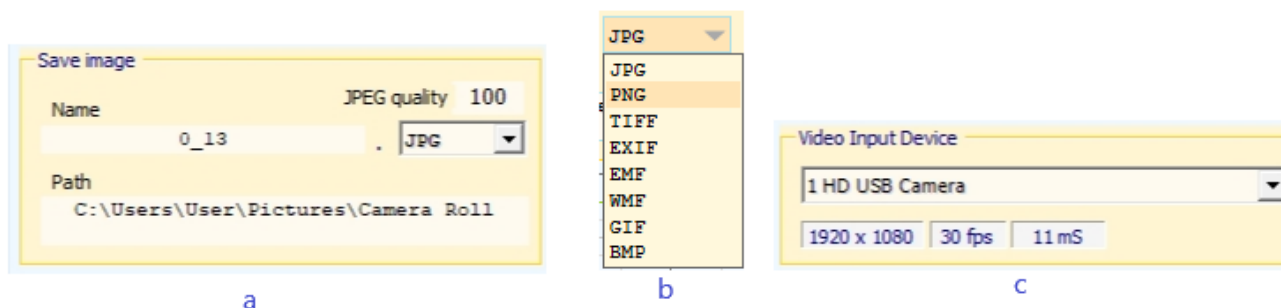


Fig. 13 a) Save image dialogue box; b) Available image formats; c) Video input device panel which shows the information about the used camera.

The save image dialogue box (shown in the figure. 13a) displays the name of the image, the storage path and the image format, which can be changed based upon the requirement. The image formats in which images can be stored are shown in figure 13 b.

3. Analysis of microstructure

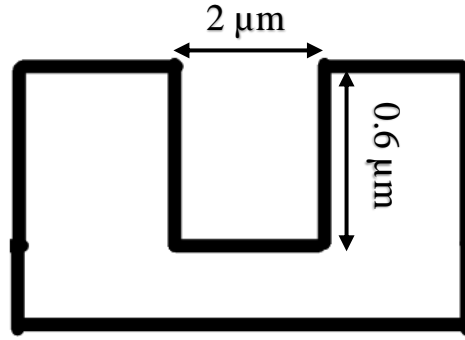


Fig. 14 Microstructure dimensions

The microchannel on which the samples are to be tested is of 2 μm width, 0.6 μm height and 20 μm length (shown in figure 14). The microchannel is embossed on the polycarbonate by the multilayer excitation of the vibroactive pad [17]. The resulting microchannel is similar to master mould [17]. The microchannel has an inlet and an outlet. The flow of the sample must be constant in order to have a concentration of the sample on the channel to be uniform (i.e. Laminar flow). If the flow is not uniform, then it may result in higher concentration at any particular point on the channel, and this may affect the result. Initially, the values of the flow rate are assumed, which is later determined based on the velocity and the nature of the flow in the microchannel. The Reynolds number(Re) has to be determined to check the nature of flow (i.e. laminar, transient or turbulent flow). The Reynolds number must be less than 100 in order to have a laminar flow in the microchannel. The flow rate (Q), from 0.25 $\mu\text{l}/\text{min}$ to 6 $\mu\text{l}/\text{min}$ are taken into consideration. A single microchannel is taken for the analysis since the velocity is the same for all the microchannels.

The velocity can be determined from the fluid flow rate [18],

$$Q = V * A$$

$$V = \frac{Q}{A} \quad (3.1)$$

Where V is the velocity, and A is the area of cross-section of the microchannel.

Width of the microfluidic channel = 2 μm = 2 * 10⁻³ mm

Height of the microfluidic channel = 0.6 μm = 0.6 * 10⁻³ mm

Where A is the area of cross-section of the microchannel [18].

Area of cross-section of the microchannel is given by

$$\begin{aligned} \text{Area of cross-section, } A &= \text{Width} * \text{Height} \\ &= (2 * 10^{-3}) * (0.6 * 10^{-3}) \\ &= 1.2 * 10^{-6} \text{ mm}^2 \end{aligned} \quad (3.2)$$

The velocity is calculated for the flow rate of 0.25 $\mu\text{l}/\text{min}$ using equation 3.1

$$\begin{aligned} \text{Velocity } V &= \frac{Q}{A} = \frac{0.25 \frac{\mu\text{l}}{\text{min}}}{1.2 * 10^{-6} \text{ mm}^2} \\ &= \frac{0.0042 \text{ mm}^3/\text{s}}{1.2 * 10^{-6} \text{ mm}^2} \\ &= 3.5 * 10^3 \frac{\text{mm}}{\text{s}} \end{aligned}$$

$$V = 3.5 \text{ m/s}$$

Now, the Reynolds number is calculated for the flow in order to find whether the flow is laminar or not. Reynolds number determines the characteristics of the fluid flow and is given by [18],

$$Re = \frac{\rho VL}{\mu} \quad (3.3)$$

Where μ is the dynamic viscosity of the fluid ($\text{kg m}^{-1}\text{s}^{-1}$); ρ is the density (kgm^{-3}), L is the characteristic length of the microchannel (mm).

$$\text{The characteristic length is given by [18] } L = \frac{4A}{P} \quad (3.4)$$

Where A is the area of the channel and P is the perimeter of the channel.

The microfluidic channel has a rectangular channel, and hence the equation becomes,

$$\begin{aligned} L &= \frac{4A}{P} = \frac{4*(W*H)}{2*(W+H)} \\ L &= \frac{2*(W*H)}{(W+H)} \\ &= \frac{2*((2*10^{-3})*(0.6*10^{-3}))}{(2+0.6)} \\ &= 0.92 * 10^{-6} \text{ mm} \\ L &= 0.92 * 10^{-9} \text{ m} \end{aligned}$$

The Reynolds number is calculated for all the three samples. The density and dynamic viscosity are given in table 2.

Table . 2 Properties of the sample [19] [20]

Sample specimen	Density ρ , kg/m^3	Dynamic viscosity μ , $\text{Kgm}^{-1}\text{s}^{-1}$
Water	997	0.001
Olive oil	911	0.1075
Glycerinum	1126	1.500

1. Water,

$$\begin{aligned} \text{Reynolds number } Re &= \frac{\rho VL}{\mu} \\ &= \frac{997 * 3.5 * 0.92 * 10^{-9}}{10^{-3}} = 0.032 < 100; \text{ Hence, the flow is laminar.} \end{aligned}$$

2. Olive oil,

$$\begin{aligned} \text{Reynolds number } Re &= \frac{\rho * V * L}{\mu} \\ &= \frac{911 * 3.5 * 0.92 * 10^{-9}}{107.5 * 10^{-3}} = \frac{911 * 3.5 * 0.92 * 10^{-9}}{1.075 * 10^{-5}} = 0.28 < 100; \text{ Hence, the flow is laminar.} \end{aligned}$$

3. Glycerinum,

$$\begin{aligned} \text{Reynolds number } Re &= \frac{\rho * V_{avg} * L}{\mu} \\ &= \frac{1126 * 3.5 * 0.92 * 10^{-9}}{1500 * 10^{-3}} = \frac{1126 * 3.5 * 0.92 * 10^{-9}}{1.5} = 2.42 < 100; \text{ Hence, the flow is laminar.} \end{aligned}$$

Similarly, the velocity is calculated for 1 $\mu\text{l}/\text{min}$, 2 $\mu\text{l}/\text{min}$, 3 $\mu\text{l}/\text{min}$, 4 $\mu\text{l}/\text{min}$, 5 $\mu\text{l}/\text{min}$ and 6 $\mu\text{l}/\text{min}$ and the corresponding Reynolds number is calculated for all the three specimens. The results are shown in table 3.

Table . 3 Reynolds number for three sample specimen.

Flow rate, Q $\mu\text{l}/\text{min}$	Flow rate, Q mm^3/s	Velocity, V m/s	Reynolds number (Re), water	Reynolds number (Re), olive oil	Reynolds number (Re), glycerinum
0.25	0.0042	3.5	0.0032	0.28	2.415
1	0.0167	13.9	0.0127	1.08	9.599
2	0.033	27.5	0.0252	2.14	18.991
3	0.05	41.6	0.0381	3.24	28.73
4	0.067	55.8	0.0511	4.35	38.54
5	0.083	69.2	0.063	5.39	47.79
6	0.1	83.3	0.076	6.49	57.53

From table 3, the Reynolds number (Re) for all the three sample specimen at different flow rates are less than 100 [18], and hence the flow will be laminar throughout the microchannel. However, the samples to be tested are incompressible fluids and have a viscous flow. The flow of the fluid is uniform throughout the microchannel, though at some particular region it exhibits maximum velocity due to the viscous flow of the liquids. The flow should be laminar for the maximum velocity in order to have a uniform concentration. The maximum velocity during the flow is calculated by simulation using COMSOL Multiphysics. A single channel is taken for analysis since the velocity is the same for all the microchannels. With the maximum velocity obtained from simulation, the Reynolds number corresponding to maximum velocity is calculated to check the nature of flow (i.e. either the flow is laminar, transient or turbulent flow).

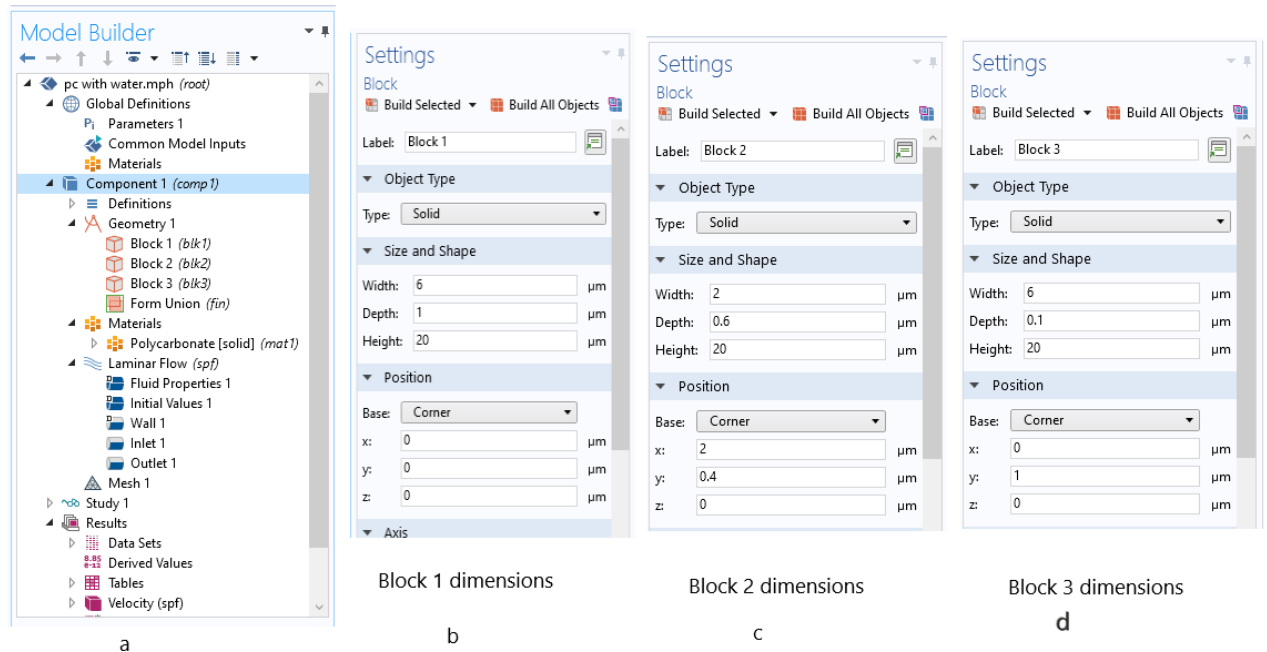


Fig. 15 a) Model builder window; b) Block 1 dimension; c) Block 2 dimension; d) Block 3 dimension.

The steps to determine the maximum flow velocity are given below,

1. A blank model is selected. Home \rightarrow 3d component \rightarrow 3D model is selected to add the 3D component. Block 1 with 6 μm width, 0.6 μm height and 20 μm length is created. Block 2 is created with 2 μm width, 0.6 μm height and 20 μm length. Block 1 and block 2 creates the microchannel for the fluid flow. Block 3 is created as a cover for the microchannel with 20 μm length, 0.6 μm height and 6 μm width. The block dimensions and the positions of the

blocks are shown in figure 15b, 15c and 15d. The Model builder window is shown in figure 15a. The created geometry using the blocks is shown in figure 16a.

2. The microfluidic channel is made of polycarbonate, and hence the polycarbonate is added to the whole component by selecting Materials (under Component 1 section) → Add material → Polycarbonate → add to the Component 1.
3. Once the material is selected, the next process is adding physics to the component. The laminar flow analysis is selected for the analysis by Physics → Add physics → Fluid flow → Single-phase flow → Laminar flow.

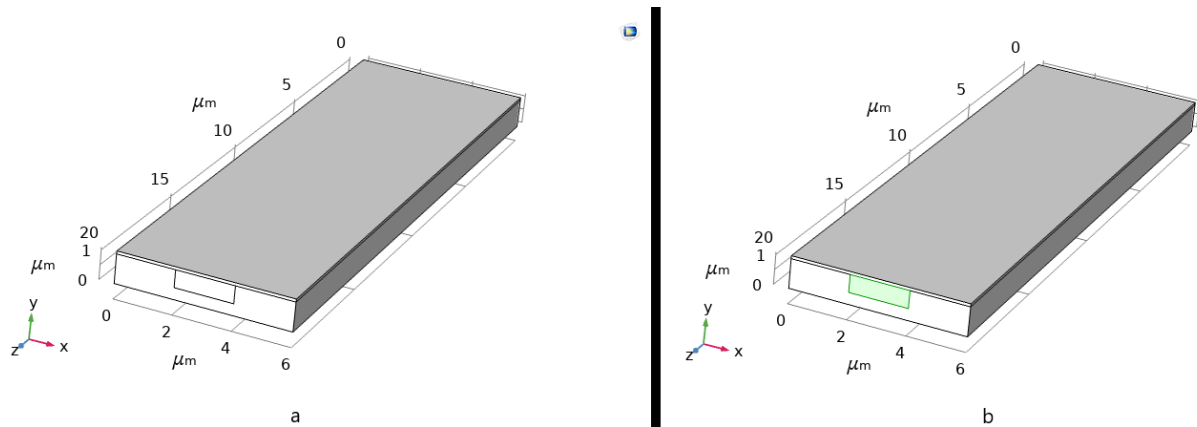


Fig. 16 a) Created geometry; b) Block 2 geometry is selected for laminar flow analysis.

4. The block 2 geometry is added for analysis in the laminar settings window under domain selection and is shown in figure 17a. The geometry selected for the analysis is indicated as green colour in figure 16b. The first sample to be tested is water, and hence the density and the dynamic viscosity of water are entered by changing to user-defined under fluid properties section (shown in figure 17b). The density and dynamic viscosity of each sample specimen are given in table 2.
5. The inlet 1 boundary is added to the physics by selecting Physics → Boundaries → Inlet. In the inlet 1 settings window, the face 13 is added to the boundary selection by selecting the face shown in figure 17c. The velocity is given as 3.5 m/s.
6. The outlet 1 boundary is added to the physics by selecting Physics → Boundaries → Outlet. In the outlet 1 settings window, the face 12 is added to the boundary selection by selecting the face shown in figure 17d.
7. The stationery study is added to the component by selecting Study → Add study → General studies → Stationery. It is added to find the distribution of velocity throughout the microchannel and the maximum velocity.
8. Then meshing is performed for the microchannel by selecting mesh under model builder and then select Build all under mesh settings window (shown in figure 18a). The channel after meshing is shown in figure 18b and 18c.
9. After meshing, the study is performed. Study 1 is selected under the model builder window. In the study settings window, select compute to perform the analysis.

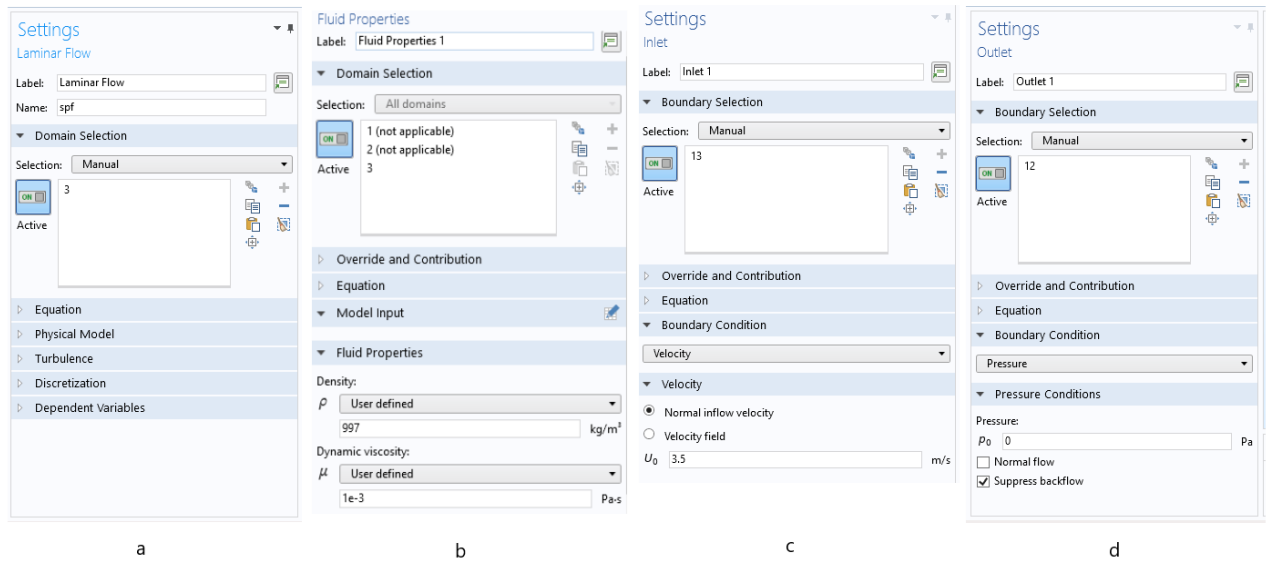


Fig. 17 a) laminar flow selection; b) Fluid properties selection; c) inlet selection; d) outlet selection.

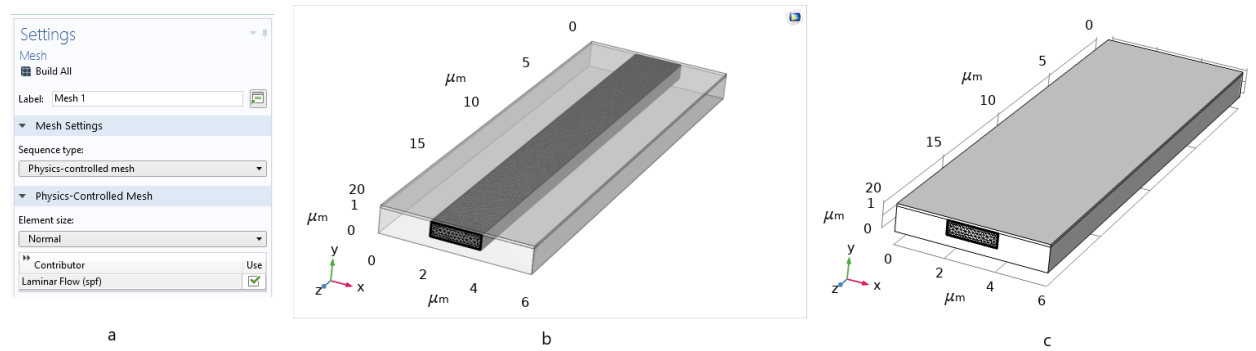
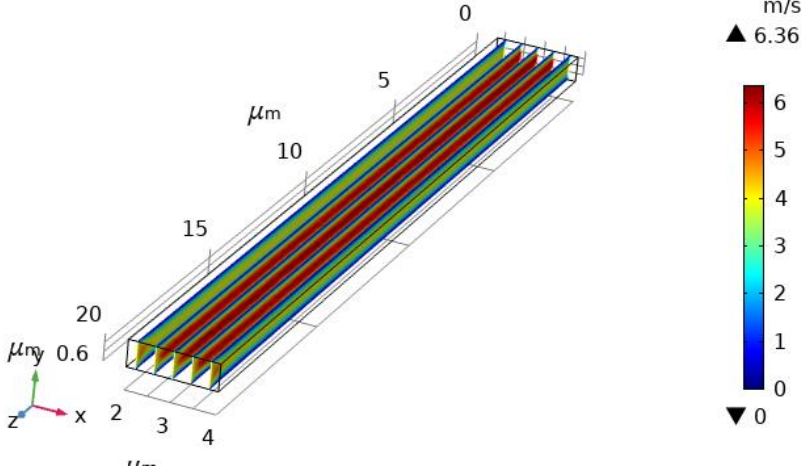
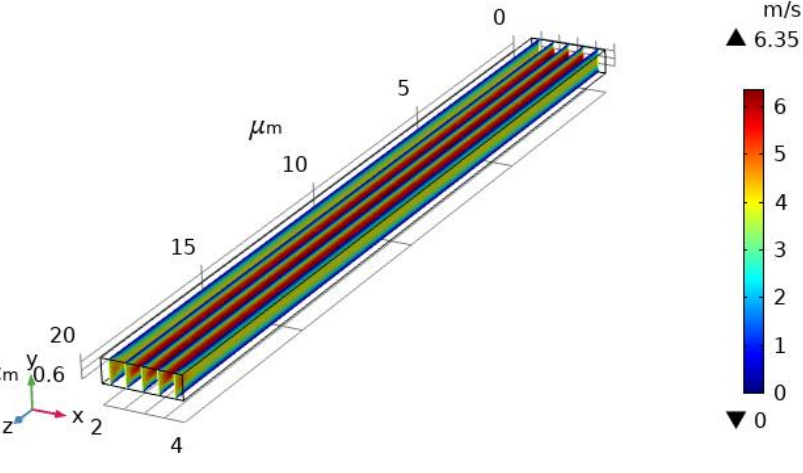
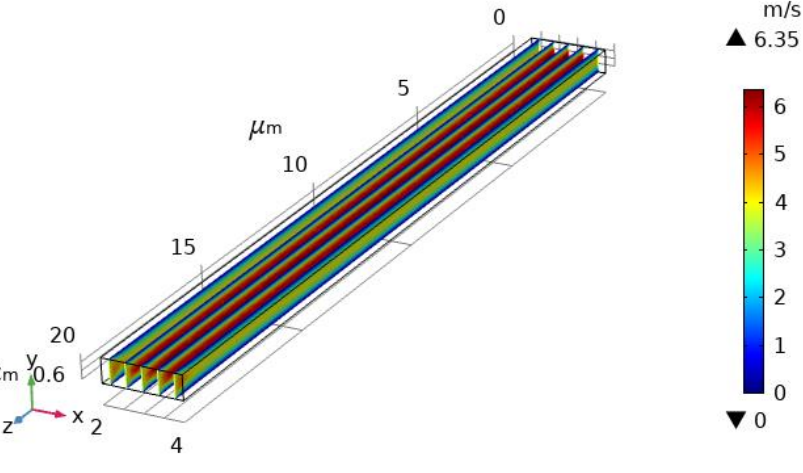


Fig. 18 a) Meshing of the laminar flow surface b) Transparent view of the mesh throughout the microchannel c) Mesh view.

10. The resulting velocity distribution of water is obtained, and the following steps are repeated to get the maximum velocity of the other two samples. The resulting velocity distribution of all the three samples is discussed below in table 4.

Table . 4 Results of simulation

Sample specimen	COMSOL Multiphysics simulation	Description
Water	<p style="text-align: center;">Slice: Velocity magnitude (m/s) water</p> 	<p>The maximum velocity of the sample on the channel is 6.36 m/s. The decrease in velocity is observed nearer to the walls of the channel, which occurs due to the friction between the water and the wall.</p>
Olive oil	<p style="text-align: center;">Slice: Velocity magnitude (m/s) Olive oil</p> 	<p>The maximum velocity of the olive oil specimen on the microchannel is found to be 6.35 m/s.</p>
Glycerol	<p style="text-align: center;">Slice: Velocity magnitude (m/s) Glycerinum</p> 	<p>The maximum velocity of the glycerinum on the microchannel is found to be 6.35 m/s.</p>

The results of the simulation for the velocity 3.5 m/s are shown in table 3, and the remaining velocities are simulated and shown in table 5.

Table . 5 Maximum velocity obtain from simulation and corresponding Reynolds number

Flow rate, Q $\mu\text{l}/\text{min}$	Velocity, V m/s	Water V_{max} , m/s	Olive oil V_{max} , m/s	Glycerinum V_{max} , m/s	Re, water	Re, olive oil	Re, glycerinum
0.25	3.5	6.36	6.35	6.35	0.005	0.495	4.385
1	13.9	25	25.2	25.2	0.023	1.965	17.403
2	27.5	49.2	49.9	49.9	0.045	3.890	34.461
3	41.6	73.8	75.5	75.5	0.068	5.886	52.141
4	55.8	97.8	101	101	0.089	7.874	69.751
5	69.2	119	126	126	0.109	9.824	87.016
6	83.3	140	151	151	0.128	11.773	104.282

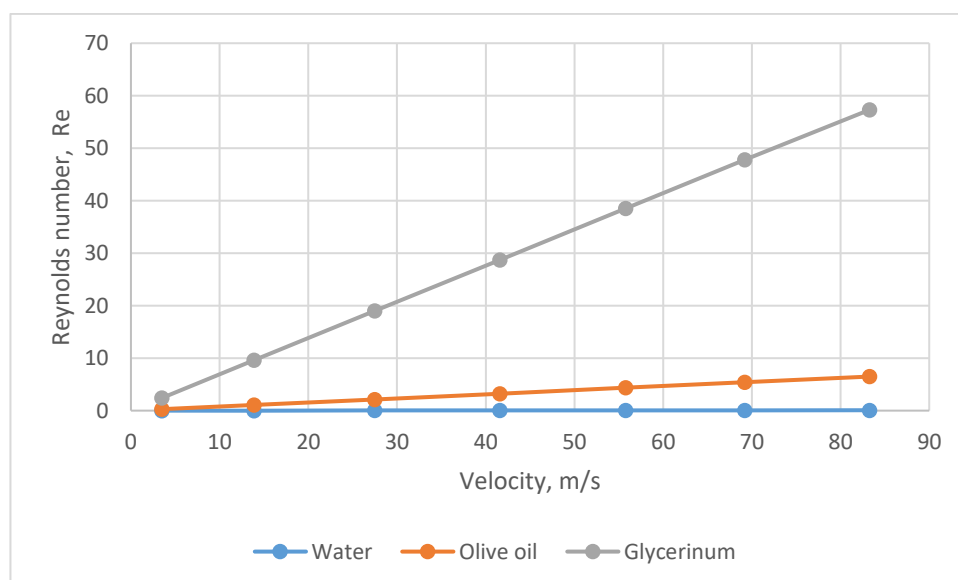


Fig. 19 Reynolds number vs Velocity

The maximum velocity during the flow is calculated by simulation using COMSOL multiphysics and shown in table 5. The Reynolds number corresponding to the maximum velocities are found using the equation, and the results are shown in table 5. From the table, it can be seen that the Reynolds number corresponding glycerinum specimen is high and are above 100 for a flow rate of 6 $\mu\text{l}/\text{min}$. Also at lower rates, the flow is laminar at maximum velocity. The obtained velocity and Reynolds number from table 3 are plotted and shown in figure 19. From the graph, it can be seen that the difference between Reynolds number of the three samples are smaller at a lower velocity (i.e. at lower flow rate) and as the velocity increases, a gradual increase in the Reynolds number of the three sample specimen can be observed. Hence, 0.25 $\mu\text{l}/\text{min}$ is chosen as the flow rate for all the three samples specimen in the microfluidic channel.

4. Construction of spectrometer

Designing of the spectrometer starts with knowing the purpose for which it has been utilised. A microfluidic channel upon which different fluids are passed is taken as the sample to be examined on the microscope. The anatomisation is further extended by the introduction of spectrometer below the sample.



Fig. 20 Nikon LV 150 microscope

The spectrometer is designed to work on NIKON LV150 microscope is shown in figure 20. The NIKON LV150 is an upright microscope which can be used for observation, inspection, research and analysis of the object under a microscope. It has wide variety of applications in various fields such as in material science for observation of properties of metals and composites; in microelectronics for analysis of wafers, observing liquid crystal displays, etc.; in optoelectronics for observing micromirror, microlenses; in biotechnology for research and analysis of various samples such as viruses, bacteria and living cells etc. Here the term microscope refers to NIKON LV150 microscope. The microscope uses LV-UEPI illuminator. NIKON LV-HL50W halogen lamp which has 50W power, is used as a light source on a NIKON LV-LH50PC lamphouse [21]. The microscope has three different magnification 5x, 20x and 100x TU Plan Fluor series magnification lenses. The main aspects to be known for experimental work are adjustment of magnification, focus and movement of the microscopic stage. Further details regarding the microscope can be found on the paper [21]. The microscope has a 3x2 microscope stage which can be moved along the X and Y axis. The microscope stage can be moved along the X and Y axis using coarse mode and fine mode. The coarse mode movement of the stage can be done by holding both stage coarse/fine movement selection switch and the stage coarse movement lever (shown in figure 21) together for movement along both X and Y axis. Pushing or pulling without holding the switch and lever will damage the stage. The fine mode movement can be done by rotating the fine movement knob for precise movement of the stage. For each X and Y axis, there exists a separate knob, as shown in figure 21. Once the positioning of the

stage is done, the next step is focusing of the specimen for further analysis. Focus can be obtained by using coarse/fine focus knobs. The knob produces the movement along the vertical direction. Using coarse focus knob, the stage moves 14 mm for one full rotation of coarse focus knob [21]. Similarly using the fine focus knob, the stage moves 0.1mm per one full rotation of fine focus knob [21]. The movement of focus knob and the corresponding stage movement are indicated along the direction is shown in figure 21.

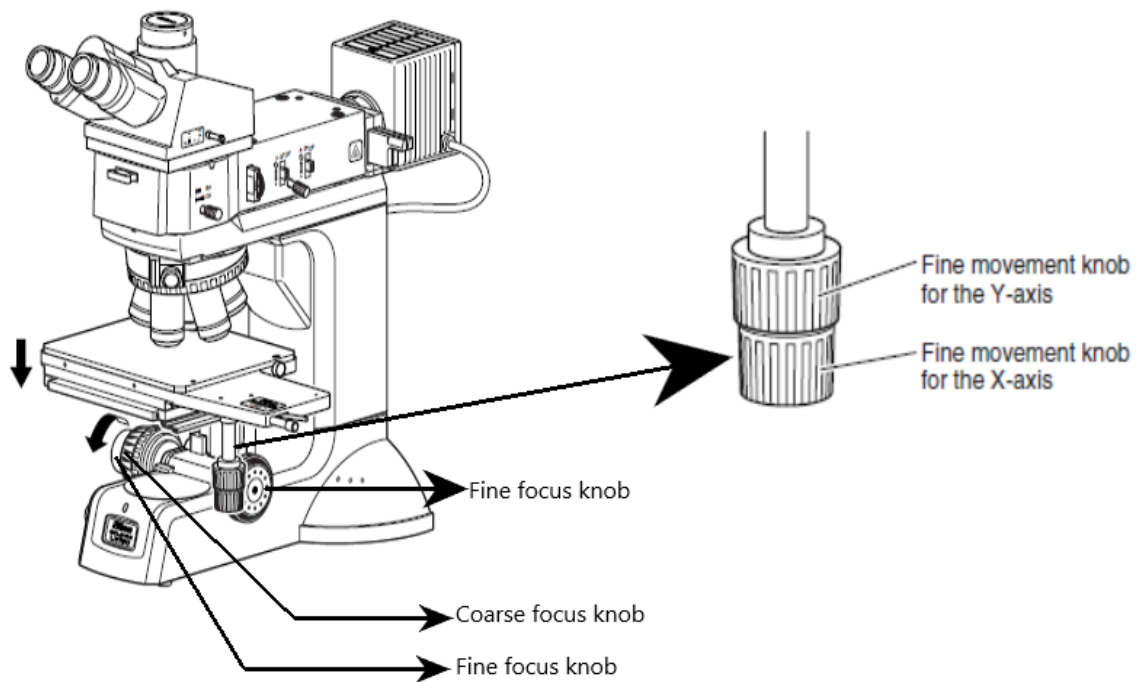


Fig. 21 Stage movement knob and focus knob for focusing the image

The microscope can be employed for various types of microscopy such as Dark field microscopy, Bright field microscopy, Differential Interference Contrast (DIC) microscopy, EPU-Fluorescence microscopy and polarisation microscopy [21]. Bright field microscopy is a basic microscopic technique in which the specimen appears darker on a bright background. While the dark field microscopy involves the viewing of the specimen, which is bright on a dark background. The sample to be tested using bright field microscopy is placed on the microscopic stage. First, the bright field mode is selected by pushing in the BF/DF button. Next, the objective lens is selected based upon the required magnification. The microscope stage is adjusted using coarse/fine movement knob based upon the requirement. Then the desired focus is achieved using the coarse/fine focus knob. Then the brightness is adjusted based upon the requirement. The binocular eyepiece is used for viewing while focusing the specimen. Once the specimen is finely focused, the specimen is captured as an image on the computer. For this purpose, the viewing mode is changed from binocular mode to photo mode using the lever. The working of dark field microscopy is similar to the bright field microscopy except that the BF/DF lever is pushed out at the start. Now, that the working of the microscope is clearly explained, and the next step is designing the spectrometer.

The position of the spectrometer is a crucial factor in determining the efficiency of the spectrometer. Before light entering the slit, it must be passed through the sample on the microscope stage. Therefore, the spectrometer must be placed underneath the microscope stage and bottom of the microscope. The region below the microscope stage and bottom of the microscope is the area of interest for the placement of the spectrometer. The space available in this region is pivotal for designing of the spectrometer, and it determines the maximum available height for the spectrometer. The sample height and its corresponding focus range need to be known approximately before determining the available height of the spectrometer. The sample to be measured are microfluids, and hence the size would be in the range of few millimetres, and focal length required for the sample will not exceed few millimetres. Hence the required height above the microscope stage is chosen as 40 mm for comfortable cushioning of the sample and also for focusing. Now, the space below the microscope stage is measured to determine the height of the spectrometer. Eliminating the 40 mm on the top, the total available height of the spectrometer is measured as 75 mm. Thus, the total height of the spectrometer should not be longer than 75 mm. The total length and width are free to be chosen, depending upon the requirement. The spectrometer construction is divided into,

1. Manufacturing of spectrometer parts.
2. Selection of camera.
3. Selection of dispersing element.
4. Final assembly of the spectrometer.

4.1. Manufacturing of the spectrometer parts

The spectrometer parts manufacturing is divided into three parts i) Main assembly box, ii) Top cover iii) Side cover. The manufacturing is categorised for assembling and further calibration of the spectrometer.

1. The main assembly has an overall width of 77mm, length of 190 mm and height of 62 mm (shown in figure 22). The thickness of each wall is 3 mm. At one end of the assembly box, a step is created by a width of 35 mm, a length of 74 mm and a height of 14 mm.

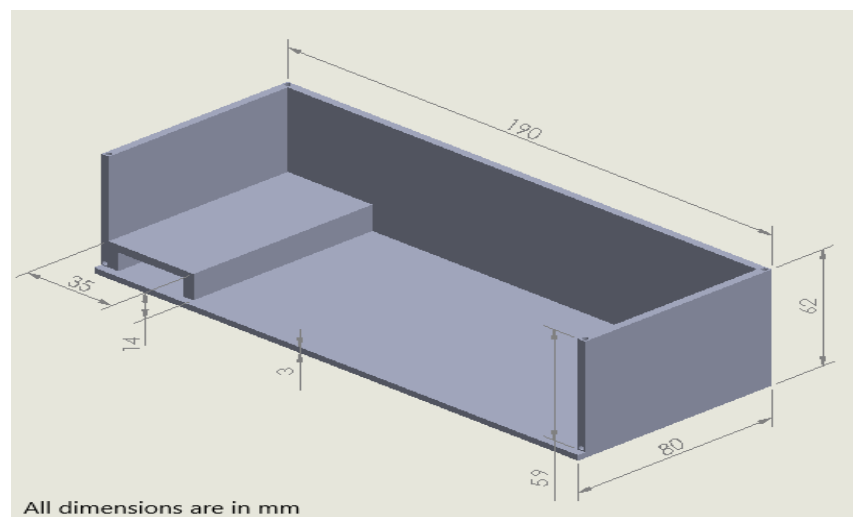


Fig. 22 The main assembly box

2. A top cover fitting the main assembly box is created with a length of 190 mm and a width of 80 mm. The top cover is shown in figure 23. On the top cover, a hole of 6 mm is created for the slit on the side same where the step is present on the main assembly box.

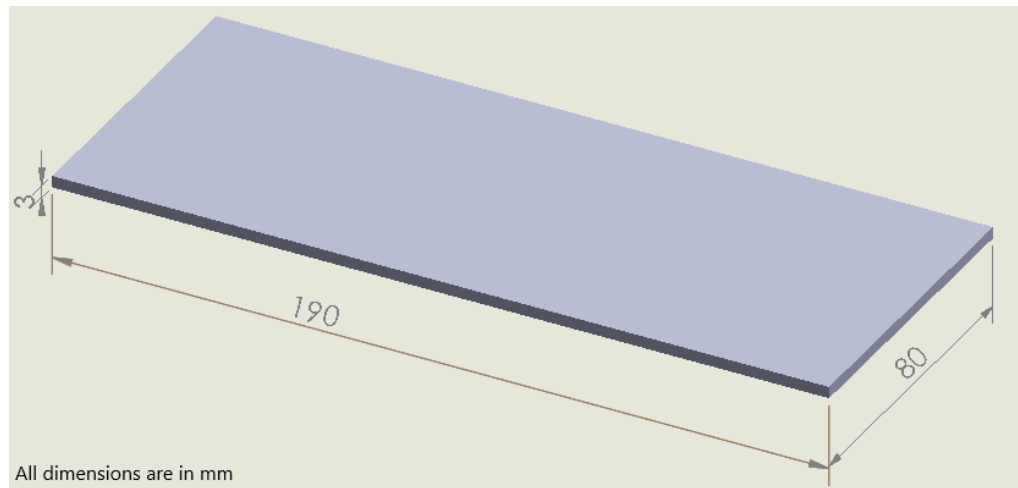


Fig. 23 Top cover for the spectrometer

3. A side cover with a length of 190 mm and a width of 59 mm is manufactured to fit the main assembly box and is shown in figure 24.

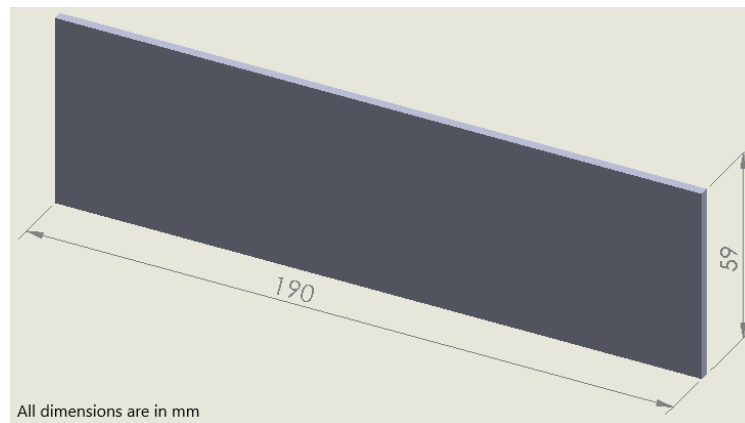


Fig. 24 Side cover for the spectrometer

A grating holder of width 40 mm and length of 13 mm and the height 15 mm is manufactured to hold the grating before the camera and is shown in appendix 1. The height of the grating holder should be the same as the height of the step created for the mirror, in order to have a straight focal plane. The parts with dimensions, as mentioned above, are manufactured using PLA material in PRUSA MK3S 3d printer. The manufacture parts are shown in appendix 2. A mirror of 50 mm width and 74 mm length is carved using a mirror cutter. Safety precautions must be taken while cutting the glass mirror.

4.2. Selection of camera

The camera required for the spectrometer should be less expensive but should have a required resolution. Generally, it is a tradeoff between the cost and resolution. The required number of pixels for the spectrometer depends on the wavelength range of the spectrometer [22]. Since visible light is the area of interest, the wavelength of the visible spectrum ranges from 380 nm to 740 nm. The number of resolution elements is $740\text{nm} - 380\text{ nm} = 360\text{ nm}$. As a rule of thumb, for each resolution element, three pixels must be allotted for each resolution element for a good resolution [22]. Hence for 360 resolution elements, the number of detector elements are $360 \times 3 = 1080$ pixels. The camera to be used for the spectrometer should have pixels approximately equal or nearer to 1080 pixels. A quick check on the internet resulted in TRUST WEBCAM 16428 camera (shown in figure 25a). The

camera has 1024 pixels which are similar to the required 1080 pixels, and the cost of this camera is very cheap compared to a camera with 1080 pixels.



Fig. 25 a) Trust web camera used in the spectrometer; b) Removal of IR filter

The camera has an infrared (IR) filter which needs to be removed. To remove the IR filter, the camera housing is removed, which is followed by the removal of the lens housing. The IR filter is present at the back of lens housing and is shown in figure 25b. The IR filter is removed carefully without any damage to the lens housing using a knife cutter. Safety precautions must be undertaken while removing the IR filter. The sensor inside the chip must be carefully protected to avoid the sensor being ruined by the dust. After the removal of the IR filter, the lens housing is fitted back to the sensor.

4.3. Selection of dispersing element

Selection of dispersing element is crucial for the efficiency of the spectrometer since it is directly related to the resulting spectrum. To obtain a spectrum, the incident light must be dispersed into wavelengths which are captured on the camera. This dispersion can be carried out using a dispersive element such as prism or grating. Prism produces spectrum only on one side and the deflection produced by the prism is not linear compared to the diffraction grating. A prism is shown in figure 26a. When exposed to white light, the emerging spectrum has a wide blue and green area, whereas, at the area near the infrared region, the spectrum is cramped. The results obtained by the prism are more difficult to calibrate and therefore, the results are not efficient. The diffraction grating, on the other side, produces more accurate spectra than the prism. Also, the cost of the prism is high compared to the diffraction grating. A grating is a tool that separates polychromatic light into its constituent wavelength (different colours) of light. In diffraction grating there exist a difference in diffraction direction. A diffraction grating is a device that consists of a continuous structure known as grooves that split light into different wavelengths of light. It is often called as “super prism” because of its efficient process of separating colours of light and have much more accurate dispersion than a prism. When the light of a particular wavelength is passed through a small structure (i.e. grooves) whose area is much smaller than the wavelength of light, then the bending of light takes place at an angle. It

is the basic principle behind the splitting of light using a diffraction grating. The factor that influences the dispersion and efficiency of the grating are i) distance between adjacent grooves and ii) the number of grooves. Increasing the number of grooves increases the resolution and decreasing the grooves reduces the resolution. Increasing distance reduces the resolution and vice versa.



Fig. 26 a) prism; b) Diffraction grating used in the spectrometer

There are two types of dispersion in a diffraction grating. They are i) transmission mode and ii) reflection mode. In reflection mode, when light is incident on the surface of the grating wavelength (colours of light) are reflected from the surface and is shown in figure 27a. In transmission mode, when a light is incident on the grating, wavelength (colours of light) is transmitted across the surface at a particular angle as shown in figure 27b. In both transmission and reflection mode, the spectrum (different colour of light) is produced on both sides (i.e. four sides) of incident light as shown in the figure 27c.

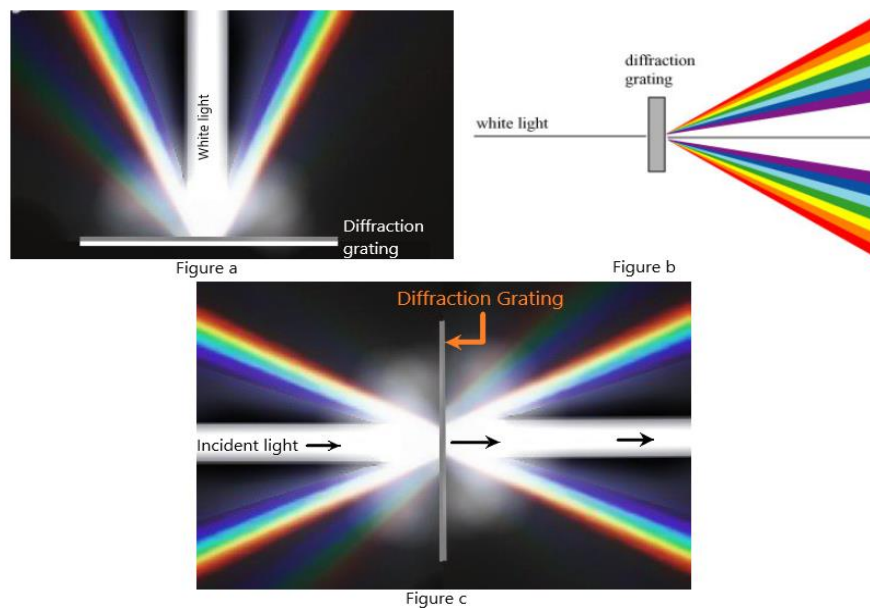


Fig. 27 a) Transmission mode of the grating; b) Reflection mode; c) Both reflection and transmission mode in the grating

The transmission mode has several advantages and produces a more accurate spectrum than the reflection mode of the diffraction grating. The reflection mode is not recommended for using in the spectrometer design due to the following reasons [23],

1. The camera must be suspended with special support for obtaining the spectrum.
2. The broadening of spectral lines occurs during the reflection mode and hence, requires a unique calibration.
3. Possibility of more stray light compared to transmission mode and results in poor resolution of the spectrum.

Hence, the transmission mode of the diffraction grating is the recommended choice for designing the spectrometer. Rainbow Symphony Diffraction grating with 1000 lines/mm is chosen as the grating element and is shown in figure 26 b. As a rule of thumb, higher dispersion is accompanied by higher the number of grooves. The selected grating is a good tradeoff between the cost and the number of grooves (lines/mm). Rainbow Symphony Diffraction grating is very cheap (i.e. few euros) compared to other commercial grating and prism.

4.4. Final assembly of the spectrometer

After the manufacture of the parts followed by the selection of camera and grating, the next step is the assembling of the spectrometer. The parts manufactured using 3d printer are grey colour, which should be painted in black colour (shown in figure 28) to avoid the scattering of light. Before painting, the parts are rubbed with 180P grit paper for smooth coating of black paint on the spectrometer parts.

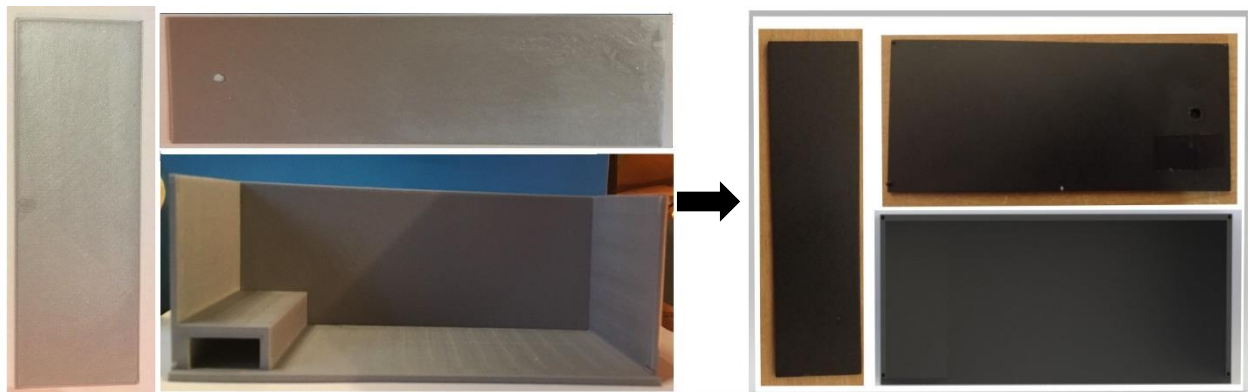


Fig. 28 Black paint given to the manufactured parts

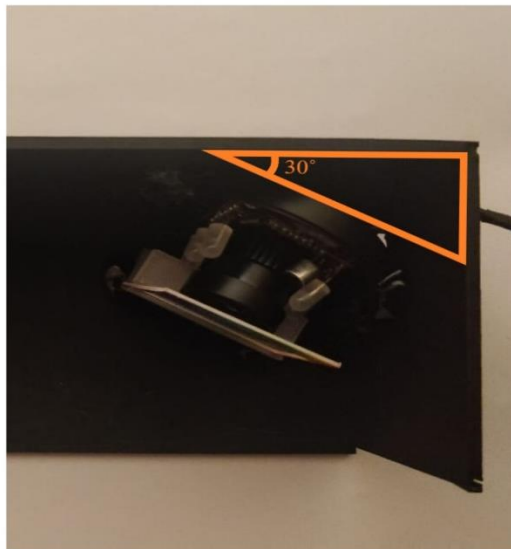
After the painting of the parts, a narrow slit has to be created on the top cover of the spectrometer. Commercial slits are accurate, although they are very expensive. A slit with 50 μm thickness and 6 mm long is created using a single razor blade and the light entering through this slit would be enough to create a spectrum. While creating the slit, it is important to have the obtain the slit straight on the hole. It can be achieved by keeping one of the blades fixed, and the other part of the blade is adjusted to achieve the linear slit. The blades are attached to the surface using an adhesive tape. The position and the final appearance of the slit, as shown in figure 32. The next process is the installation of the camera on the assembly box. The chosen Trust Webcam must be fixed at a position to obtain the spectra from the grating. The camera is placed on the other side of the box, as shown in figure 31 opposite to the mirror. The position of the camera on the box is pivotal to obtain a good spectrum. Table 6 indicates the angle at which a particular wavelength is observed. The formula for calculating the deflection of a particular wavelength(λ) [23] is given by,

$$\text{Deflections in degrees} = \arcsin \left[\frac{\lambda}{\text{Line spacing (nm)}} \right] \quad (4.1)$$

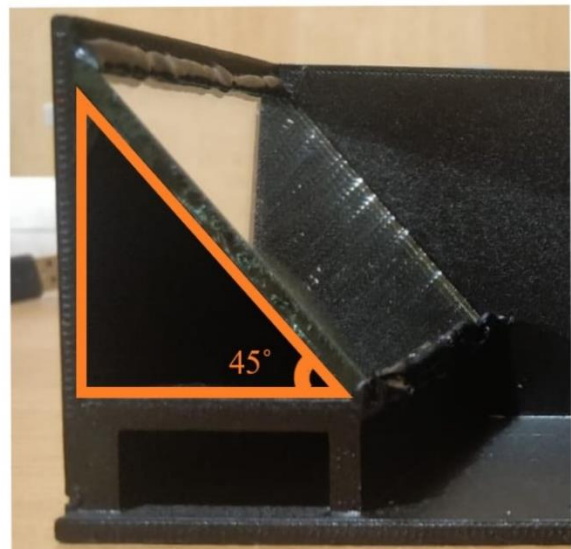
At angles between 24° and 44°, the required visible light is observed. The angle 30° is at the centre for the selected visible light range. This position is selected as the angle of placement for the camera. Hence, the camera is positioned at an angle of 30° for a good compromise between resolution and amount of light collection. Usually, the variation of angle ranges from 20° to 45°. The grating placed on the grating holder is placed precisely in front of the camera. For good resolution, the camera angle is maintained at 30° and is shown in figure 29a. A hole is created near to the camera assembly for a USB port. The USB is attached to the computer to obtain the spectrum on the thermino software.

Table . 6 Deflection in degrees

Type of grating	Lines per mm	Line spacing, nm	Deflection degrees for various wavelength				
			400 nm	500 nm	600 nm	700 nm	800 nm
Diffraction grating	1000	1000	24	30	37	44	53



a



b

Fig. 29 a) Position of the camera ;b) Position of the mirror

Focusing the light on to grating is the core part of fixing the mirror on to the box. Before positioning the mirror, it is essential to know the fact that the focal length of the mirror is infinite. The light enters the spectrometer in a vertical direction which needs to be bent to a horizontal direction. For focusing the light, the mirror needs to be tilted at an angle such that the ray strikes the grating. When the mirror is tilted at an angle of 45°, the light exactly focuses on the grating, which is on the horizontal direction. The position of the mirror is shown in figure 29b. A schematic diagram representing the light ray entering the slit is passed through the mirror and reaches the camera is shown in figure 30. Before glueing all the parts at a fixed position, a bench test is performed to check the efficiency of the spectrometer. The camera is attached to the computer, and the results are obtained using thermino software. The experiment is performed using the warm white led on the spectrometer and spectrum of the white led is obtained. The result of the bench test is shown in appendix 3.

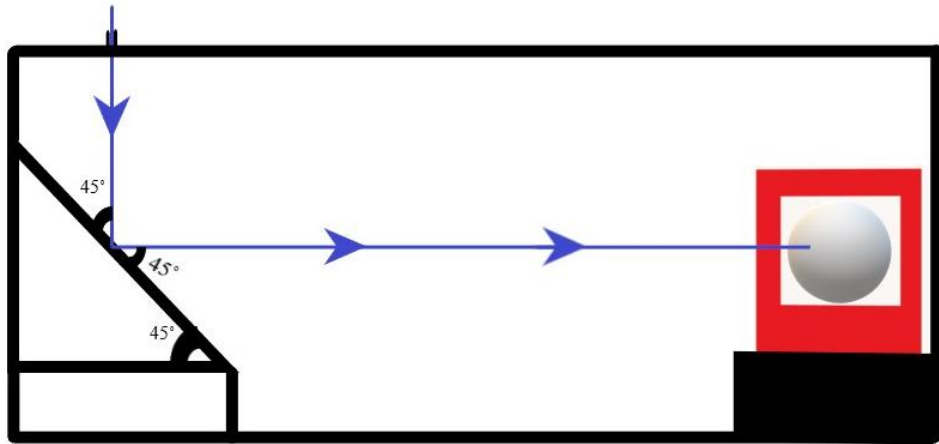


Fig. 30 Flow of light inside the spectrometer

After the bench test, the parts of the spectrometer has to be fixed such that it will remain in the exact position. The mirror of 50 mm long has to be fixed at an angle of 45° on the step created on the box using a hot glue gun. Similarly, the camera and the grating are fixed on the exact position using the hot glue gun, and the assembly box would appear, as shown in figure 31.



Fig. 31 Full view inside the spectrometer.

Once all the parts are fixed on the position, again a bench test is performed to check the result of the spectrometer. Once the test is done, the final assembling of the spectrometer must be finished. First, the top cover is fixed on to the main assembly box. While fixing the top cover, it is essential to have the slit in position to obtain the spectrum. The top cover is attached to the main assembly box using the hot glue gun. Next, the side cover is attached to the main assembly box using a hot glue gun. After glueing all the parts, the final appearance of the spectrometer is shown in figure 32.



Fig. 32 Assembled visible light spectrometer

5. Experimental setup

After the construction, the spectrometer is now ready for testing. The objective of this project is to perform two kinds of real-time analysis when a sample is placed under the microscope. The sample that is to be tested is placed on the microfluidic channel network. The microfluidic channel is embossed on a sheet of polycarbonate. The microfluidic channel has a number of fluid channels with an inlet and outlet. The schematic representation of the microfluidic network to be tested is shown in figure 33.

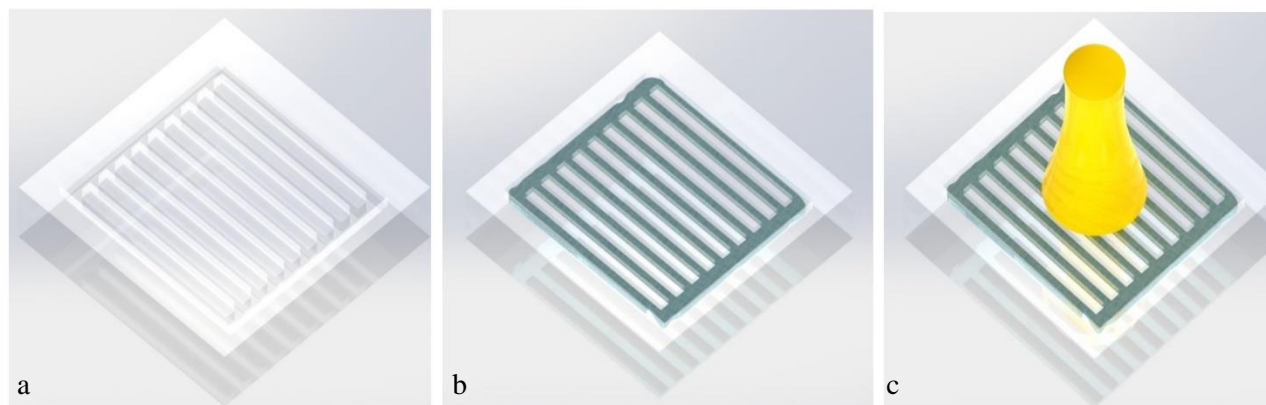


Fig. 33 Microfluidic channel network

Fig. 33 a) Shows the microfluidic channel network made of polycarbonate material; b) shows the channel with fluid flowing from inlet till outlet; c) shows the light from the source passing through only a specific area on the channel.

The sample is tested over a range of microfluidic channels which lies on the entire light diameter. The light is illuminated on the microfluidic channel network for a 6 mm diameter. So, the microfluidic channels and the sample specimen present in this region is only exposed to the spectrometer.



Fig. 34 The green laser and red laser used for calibration

The spectrometer performance has to be tested in order to check the efficiency. First, the spectrometer is tested, which is followed by an experimental setup for detection of bio-particle. For the test experiment, the spectrometer is tested with a red and green laser. The wavelength of the red laser as prescribed on the device is 650 ± 10 nm and is shown in figure 34. Similarly, the wavelength of the green laser, as mentioned on the device is 532 ± 10 nm (shown in figure 34). The spectrometer camera is connected to a PC via USB cable. The resulting spectrum is observed using the thermino software. The green laser is illuminated through the slit, and the resulting spectrum is observed in the thermino software. The maximum peak corresponds to the maximum transmitted wavelength. The observed spectrum has only green colour, and its corresponding wavelength is 550 nm and is shown in figure 36. The required wavelength of 532 ± 10 nm is not achieved, although green light is observed in the image. The spectrometer needs calibration to obtain the required wavelength (i.e. 532 ± 10 nm). The calibration can be done in the software. The calibration is done by altering the peak points. The software has its own trim points for calibration, which can be used only with fluorescent spectrum. The calibration in this experiment is done with the green laser. The steps for the calibration are,

- i) Before starting the calibration, make sure that the reference and peaks are pressed.
- ii) After the spectrum of green laser is obtained, select Tools → Trim points → Select trim points manually (shown in figure 35).
- iii) Enter the first reference point as 528 nm.
- iv) Press Trim scale on the bottom and make sure the entered reference peak appears on the label section.
- v) Hold the left mouse button on the label section and gently move the peak at 550 nm towards the reference peak of 528 nm.
- vi) Once the required peak of 528nm is achieved (shown in figure 37), the calibration of the spectrometer is completed.

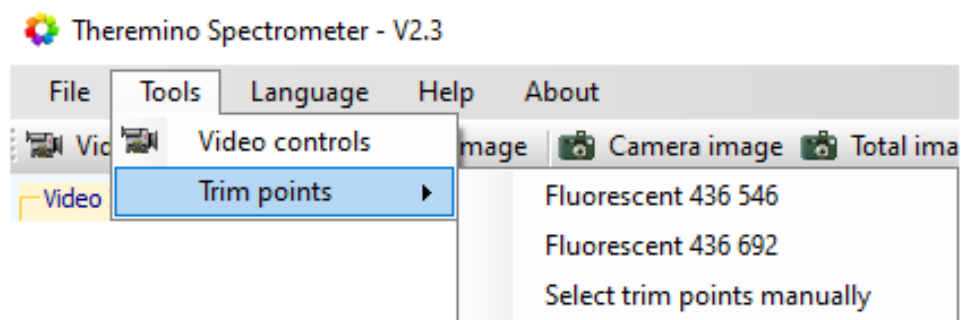


Fig. 35 The path to select trim points

In fig 35. The software has its trim points which can be used with a fluorescent spectrum.

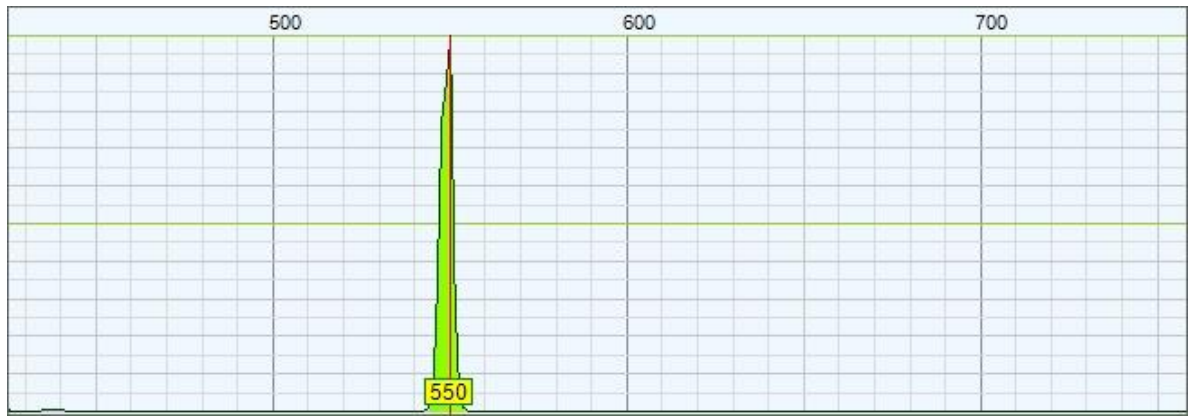


Fig. 36 Spectrum of the green laser without the calibration.

The maximum peak corresponds to the maximum transmitted wavelength. Once the calibration is done, again the spectrometer is checked with the red laser to check its efficiency after calibration. The observed spectrum shows the maximum peak at 632 nm, which is approximately equal to 650 ± 10 nm of the red laser. The obtained spectrum of red laser is shown in figure 38. The bench test proves the designed spectrometer to be efficient. Now the next step is assembling of the spectrometer on to the microscope. The microscope stage is raised to maximum height in an upward vertical direction. Then the spectrometer is placed below the microscope stage, as shown in figure 39. The position is adjusted to focus the light on the slit. The spectrometer is placed on the microscope with USB of the camera being connected to the computer. The microscope is connected to a PC to record the observed specimen. The microscope stage is lowered for placing the sample on it. The experiment is carried out with three types of samples being placed on the microscope stage. They are i) Olive oil ii) Glycerinum iii) Water. These samples are chosen because these liquids are used as a solvent material for the analysis of bio particle.



Fig. 37 The spectrum of green laser with a peak at 528 nm obtained after calibration.

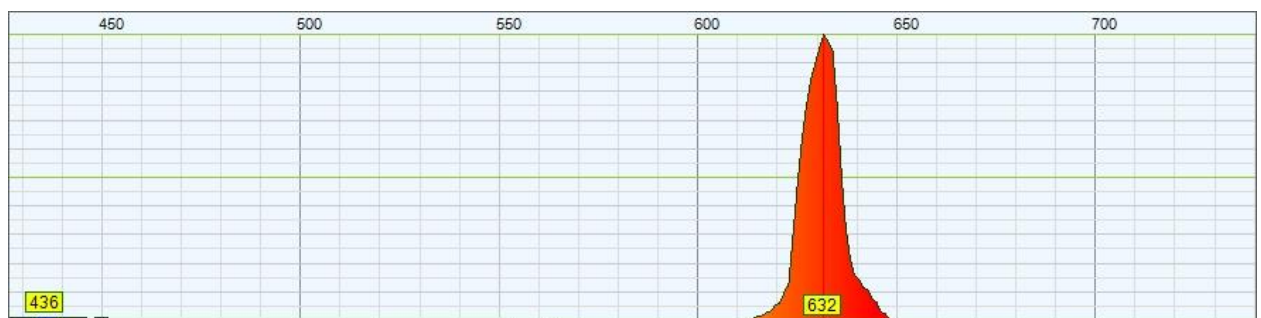


Fig. 38 The spectrum of red laser with a peak at 632 nm

The entire experimental setup is shown in figure 39. There are four steps for detecting the particle present in the given samples are,

1. Firstly, the light from the microscope is illuminated onto the spectrometer. The resulting spectrum is recorded on the computer using thermino software.
2. Secondly, the polycarbonate is placed on the microscope stage, and then the objective lens and the stage is adjusted till a finely focused microscopic image is observed. The corresponding spectrum of polycarbonate is observed. The results of the microscope and spectrum are obtained. In order to find the spectral difference between the polycarbonate and microfluidic channel embossed on polycarbonate, the spectrum of polycarbonate is recorded.
3. Thirdly, after recording the polycarbonate spectrum, the microfluidic channel is observed, and the microscope image is obtained. The corresponding spectrum is observed, and both the results are recorded on the computer.
4. Fourthly, the first sample to be tested is olive oil injected out onto the microfluidic channel, and the microscope stage and the objective lens are adjusted till the microscopic image is clearly focused. The resulting spectrum is observed, and the results are recorded on the computer. Similarly, the other two samples, i.e., glycerinum and water, are tested. The corresponding microscopic images and the spectrum images are recorded on the computer.

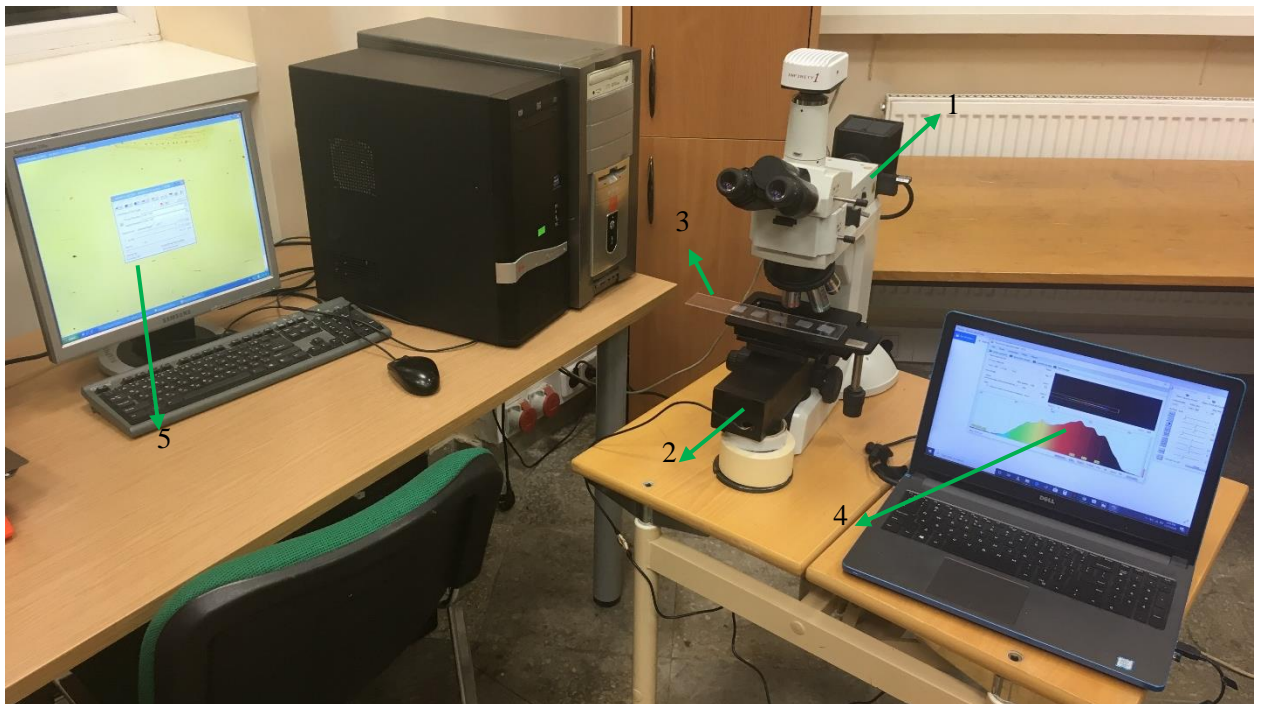


Fig. 39 The entire experimental setup

In Fig.39 1) Denotes the microscope; 2) The spectrometer placed under the microscope stage with light from the source is focused to the slit; 3) The sample specimen which is to be tested; 4) Resulting spectrum displayed in the Thermino software; 5) The microscopic image on the computer

6. Results and discussion

The experiment is carried out according to the procedures, and the results are being obtained. The light source used in the microscope for the experiment is NIKON LV-HL50W halogen lamp. With the spectrum of individual samples, it is very difficult to determine the presence of absorbance, transmittance and peaks since the light has to be passed through multiple layers before reaching the spectrometer. Each layer has its own absorbance, transmittance and peaks, which varies due to different characteristics of each layer. Here the term sample spectrum refers to the spectrum obtained from the three individual sample spectrum, i.e. olive oil spectrum, water spectrum and glycerinum spectrum. The sample spectrum is compared with the spectrum of the individual layers, and by comparing the difference in the spectrum of individual layers, the transmittance, and peaks produced by the specimen can be determined. The spectrum of the halogen lamp light source is obtained and is shown in figure 40. The intensity of the light is kept constant.

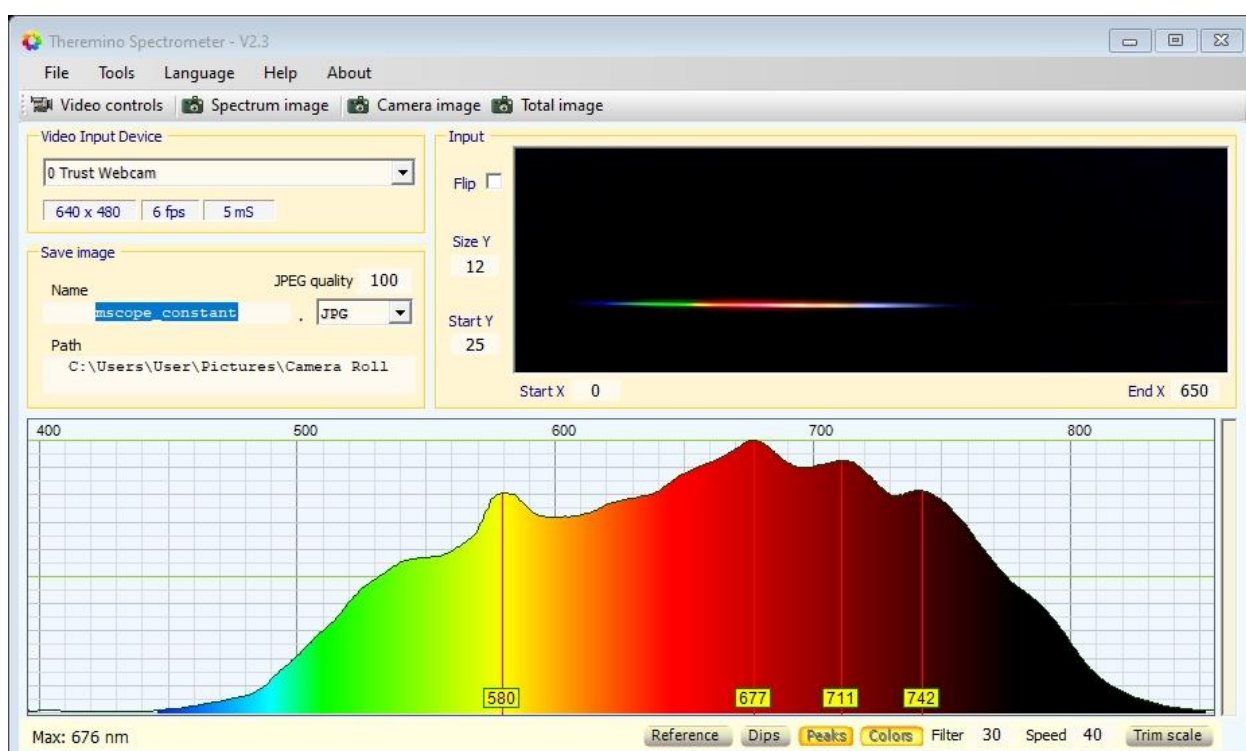


Fig. 40 Spectrum of the microscope light (halogen lamp)

The spectrum of the polycarbonate on which the microfluidic channel network is embossed is shown in figure 41. From the figure, the spectrum of polycarbonate is similar to the spectrum of halogen lamp since the polycarbonate is transparent and does not absorb any light. The microscopic image of the polycarbonate material is shown in figure 42a.

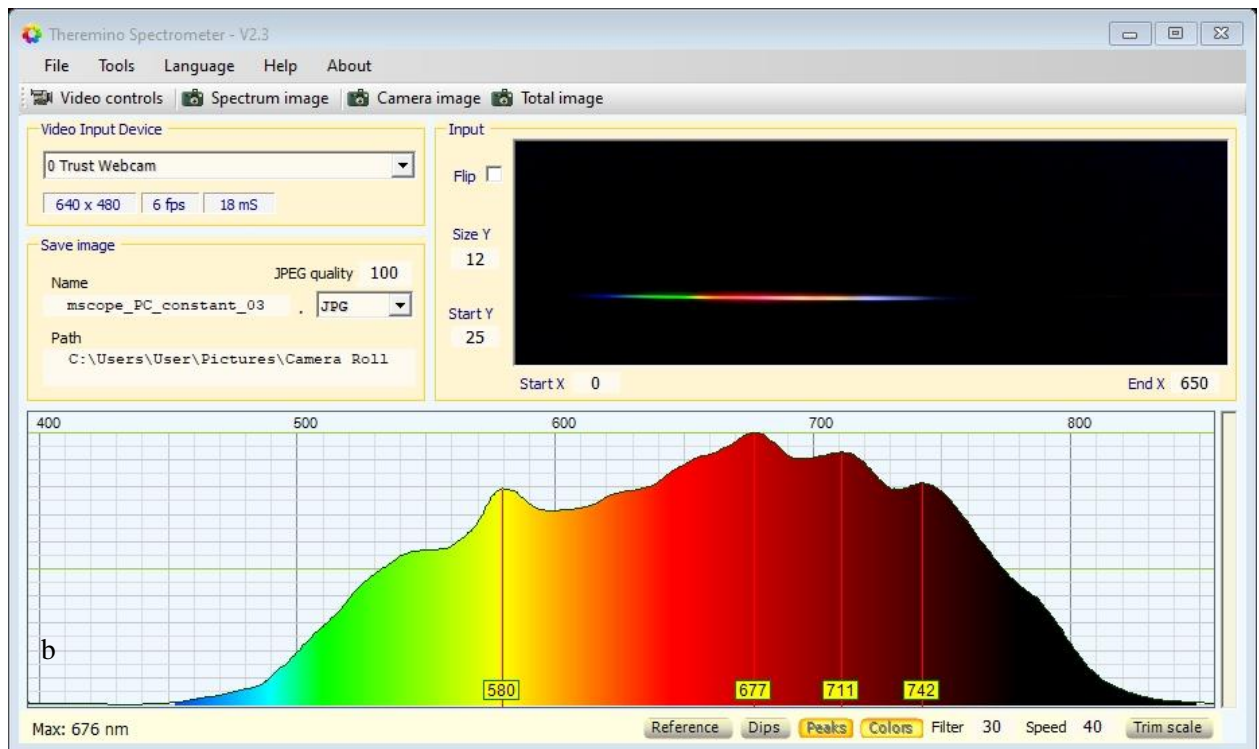


Fig. 41 Spectrum of the polycarbonate material.

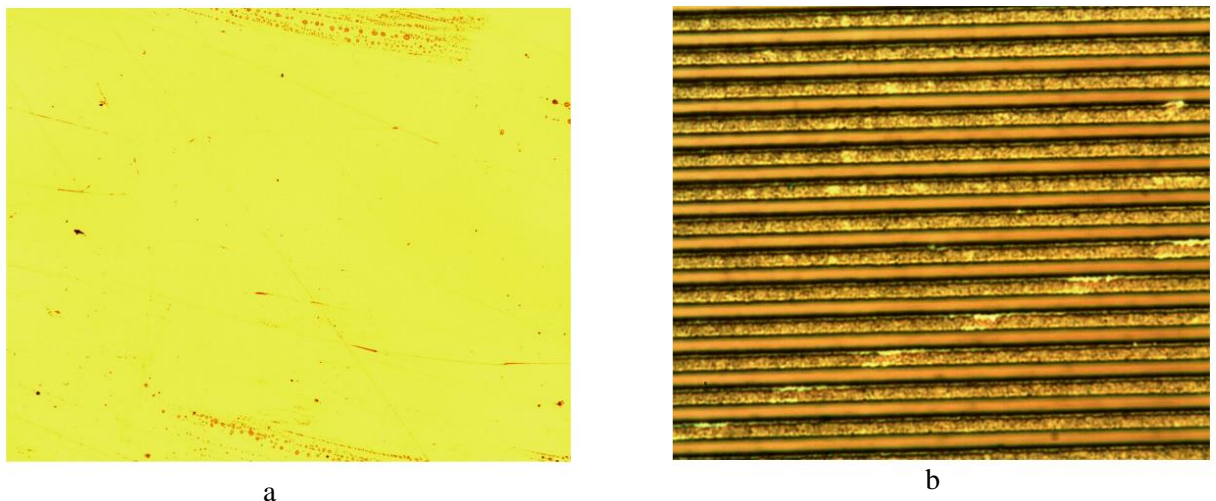


Fig. 42 a) Microscopic image of polycarbonate; b) Microscopic image of the microfluidic channel network

The spectrum of the microfluidic channel network embossed on the polycarbonate is shown in figure 43. This spectrum is taken as the reference spectrum for the interpretation of the sample spectrum. From the microfluidic channel network spectrum, an increase in absorbance is observed at the greenish-yellow region. A sharp increase in absorbance is found in the yellow region. This is because of the consecutive distance between the channels [24]. 1000 μm are present in 1mm [24]. The period of a microchannel in the microstructure is 4 μm and hence, $1000/4 = 250$ lines/mm. This corresponds to the blue line (i.e. 300 grooves/mm) shown in figure 44. The blue line has an increase in absorbance near 500 nm. This is the reason for the decrease in transmittance in the spectrum of the microfluidic channel network at 500 to 600 nm. The decrease in the transmittance is due to the small period of channels in the microfluidic channel network. The corresponding microscopic image is shown in

figure 42b. From figure 42b, the microfluidic channel walls are properly embossed and have a good surface roughness compared with the channel produced by other manufacturing techniques.

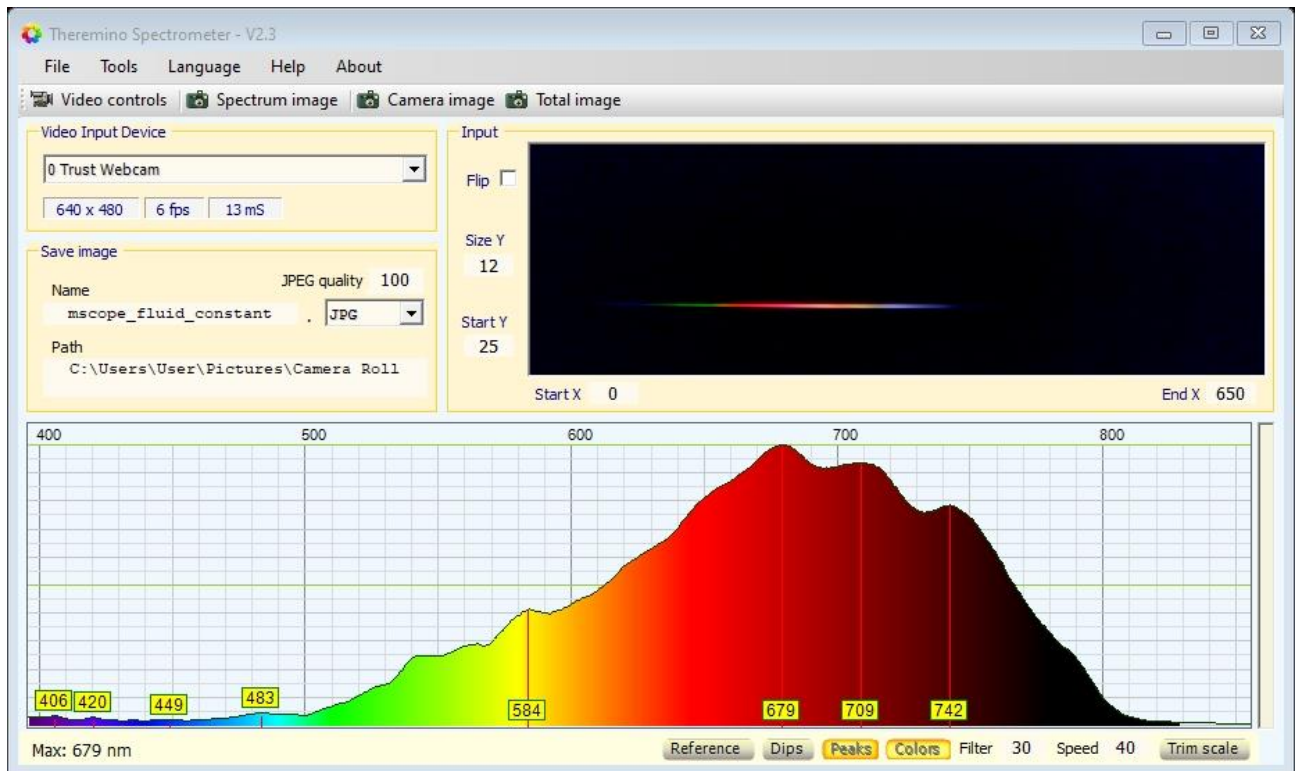


Fig. 43 Spectrum of the microfluidic channel network.

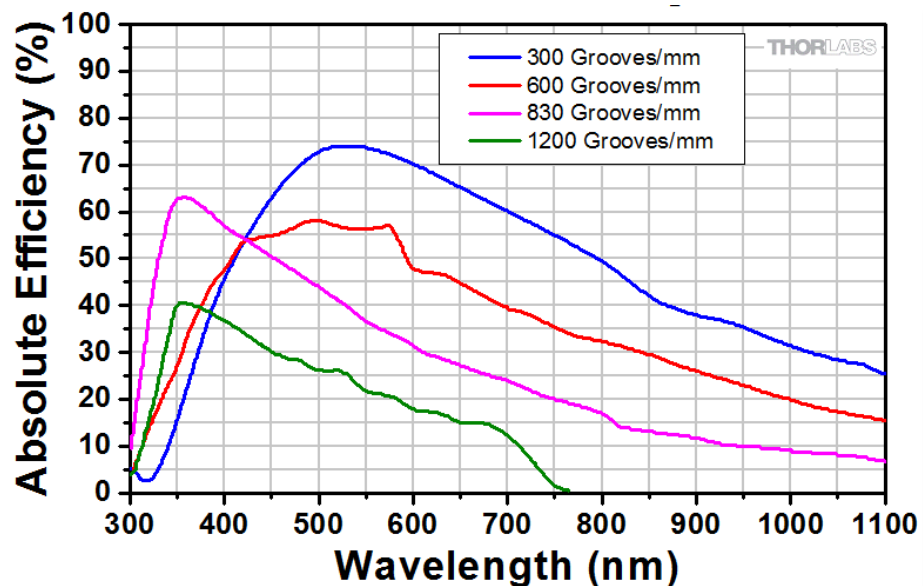
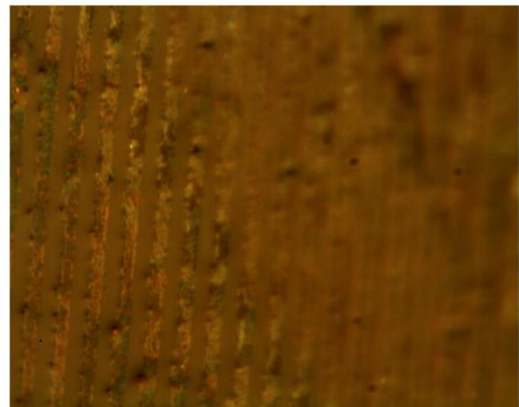
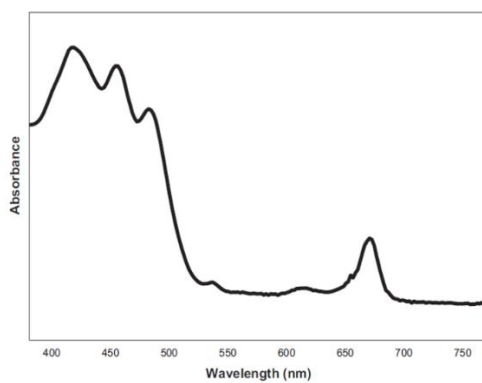


Fig. 44 Absorbance caused by the period of the microstructure [24]

6.1. Olive oil spectrum

The spectrum of the olive oil on the microfluidic channel network is shown in figure 46. Here the sample spectrum refers to the olive oil spectrum. The sample spectrum is compared with the reference spectrum, and a peak at 544 nm is observed in the greenish-yellow region. When taken absorption

spectrum of olive oil into consideration, (shown in figure 45 a) maximum absorption can be observed from 400 nm – 500 nm, which can also be seen in the sample spectrum. Also, the peak in the green-yellow region (at 546 nm) denotes the presence of a chlorophyll B pigment in the sample, which absorbs light at 410-480 nm and emits light in the greenish-yellow region. Olive oil contains pigments like chlorophyll A, chlorophyll B and carotenoids [25]. Hence, it can be noted that, out of the three main pigments in olive oil, chlorophyll B pigment is exceedingly present in the sample, which is responsible for the greenish-yellow colour. The colour of olive oil depends upon the intensity of pigment largely present in it, which varies upon the climatic conditions, fertilisation and the manufacturing process of the olive oil [25]. The microscopic image of the olive oil specimen is shown in figure 45 b.



a

b

Fig. 45 a) Absorbance spectrum of olive by Dr.Cosimo et al. [25]; b) Microscopic image of olive oil

From fig 45 a) The absorption of olive oil has a sharp decrease at 540 nm to 550 nm which is also observed in the olive oil spectrum obtained from the visible light spectrometer, shown in figure 46.

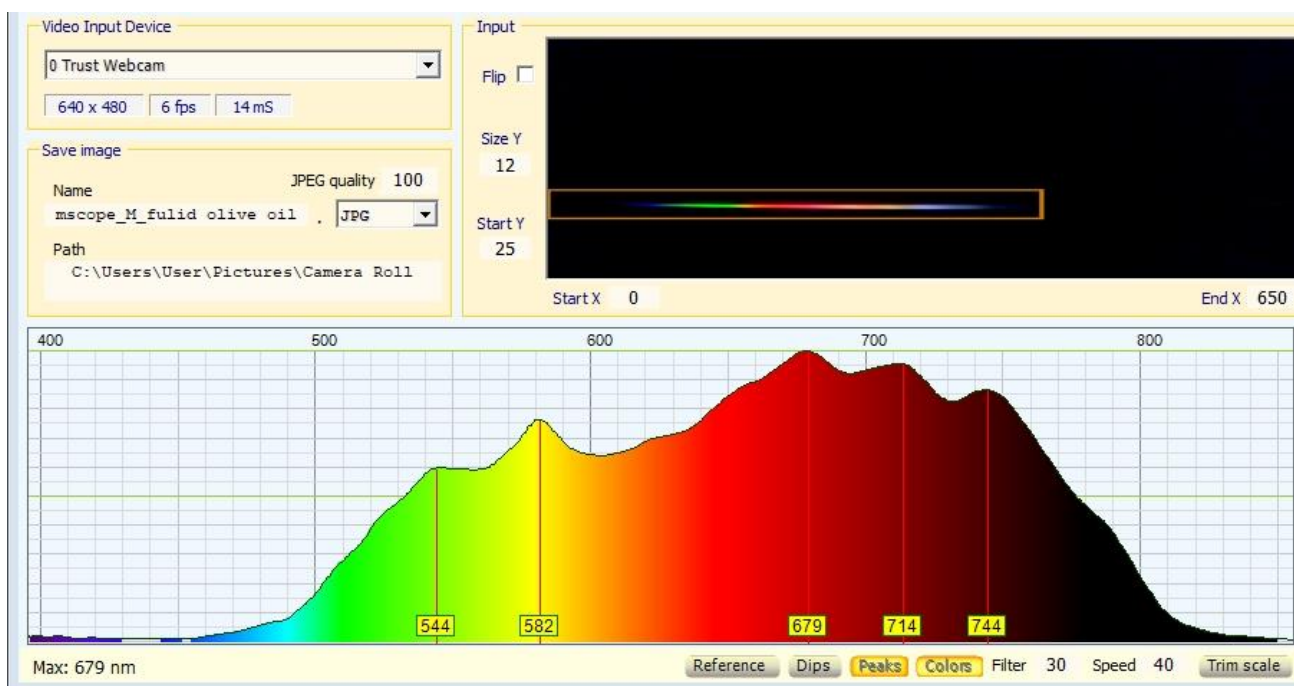


Fig. 46 Spectrum of the olive oil

6.2. Glycerinum spectrum

The spectrum of the glycerinum on the microfluidic channel network is shown in figure 47. The microscopic image of the Glycerinum sample on the microfluidic channel network is shown in figure 48b. The glycerinum spectrum is compared with the reference spectrum. From glycerinum spectrum, it can be observed that the peak is formed at 560 nm after the placement of glycerinum on the microfluidic channel network. The absorption spectrum (shown in figure 48a) shows that the molecule of glycerinum has a constant absorbance in the visible region, which is quite low since it is transparent [26]. Due to this, the transmittance is high in the visible region and the same can be observed in the Glycerinum spectrum observed from the design visible light spectrometer. Glycerinum has a high transmittance, which is the reason for the formation of the peak in the Green-Yellow region when compared with the reference spectrum.

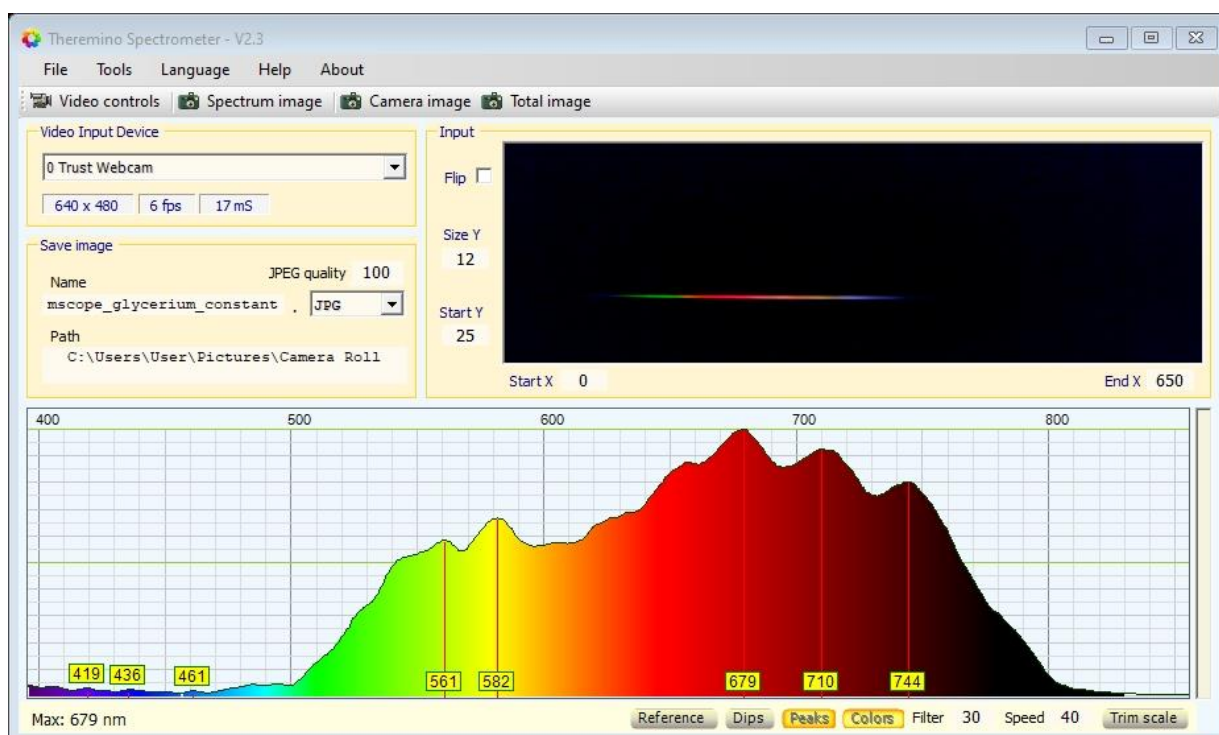


Fig. 47 Spectrum of the glycerinum obtained from the spectrometer

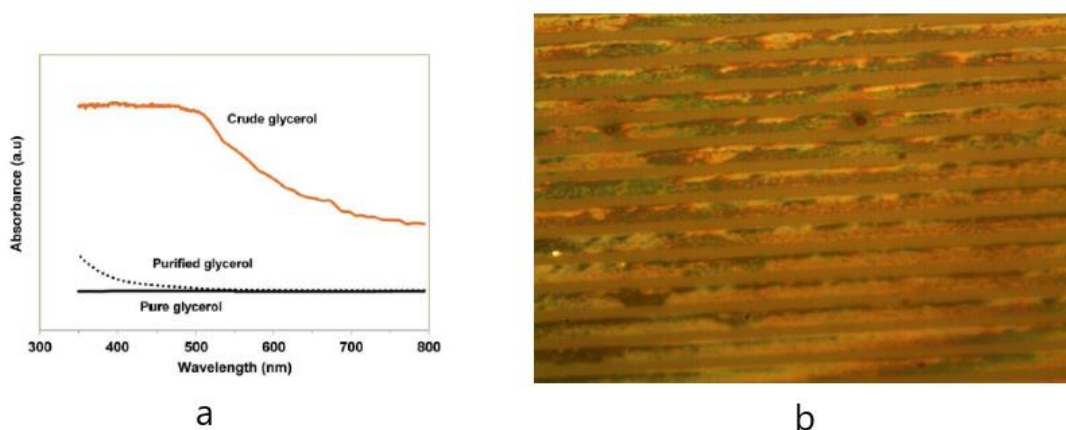


Fig. 48 a) Absorbance of glycerol spectrum [26]; b) Microscopic image of glycerinum

Fig 48a. Shows absorbance of pure glycerinum is very low, and the absorbance tends to increase with an increase in impurities. This gives the conclusion that glycerinum has a high transmittance in the visible region, which can be seen in the glycerinum spectrum (shown in figure 47) obtained by the developed visible light spectrometer.

6.3. Water spectrum:

The water spectrum shown in figure 49 is compared with the reference spectrum. It can be observed that there is an increase in transmittance in the green-yellow region compared to the reference spectrum. The water spectrum obtained from the spectrometer is compared with the absorbance spectrum of the water shown in figure 50 a. Water absorbs light in ultraviolet, infrared and in the far infrared region and transmits light in the visible the region [27]. At 760 nm-800 nm, a strong transmittance can be observed in the reference spectrum, and a decrease in the transmittance is noted in the water spectrum. This change in the water spectrum takes place because water molecules absorb light in the infrared and far infrared region. The microscopic image of the water specimen on the microfluidic channel network is shown in figure 50b.

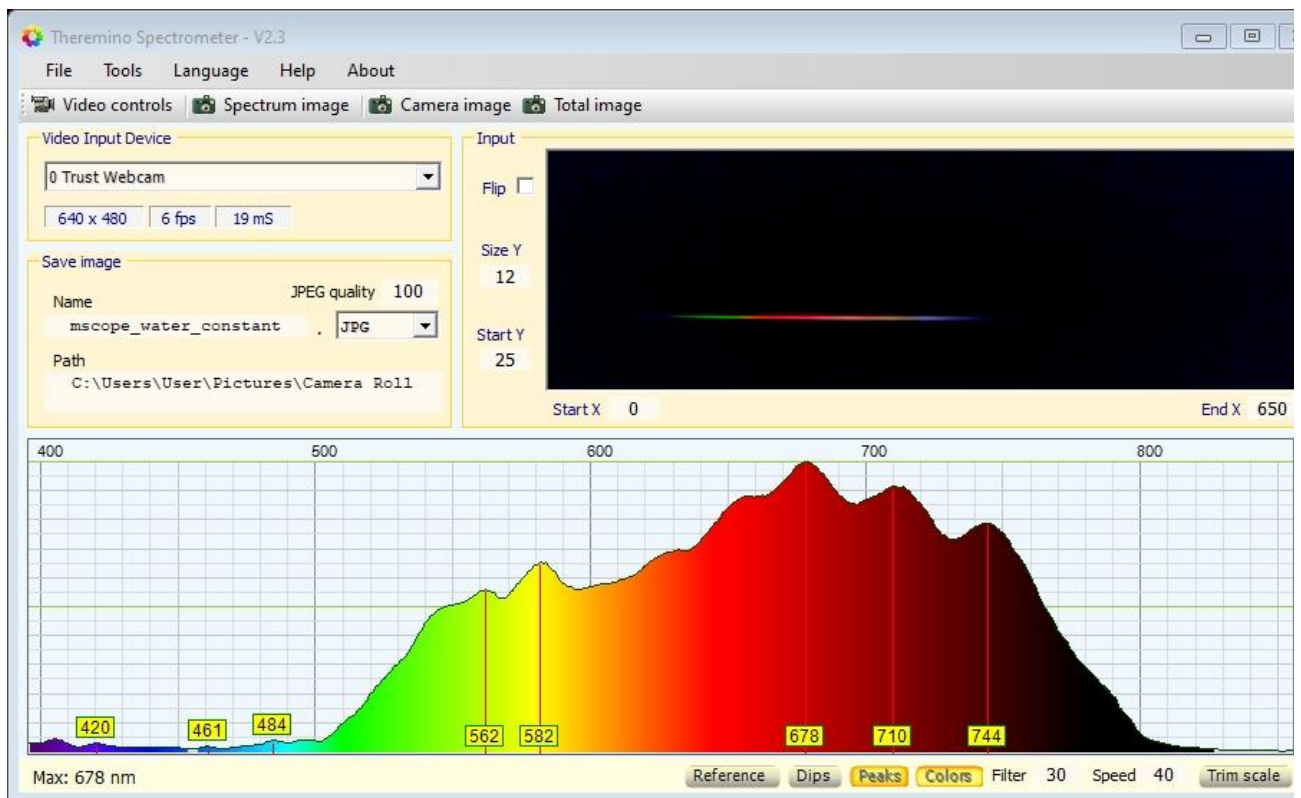
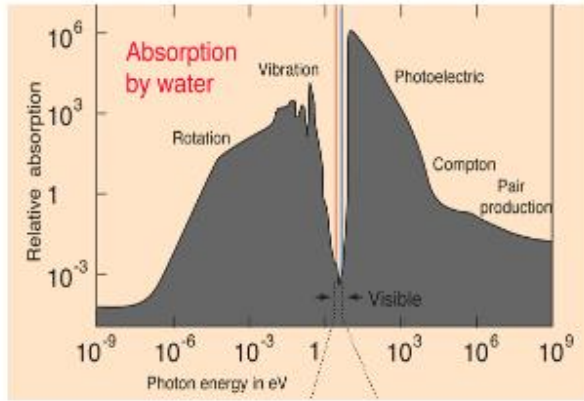
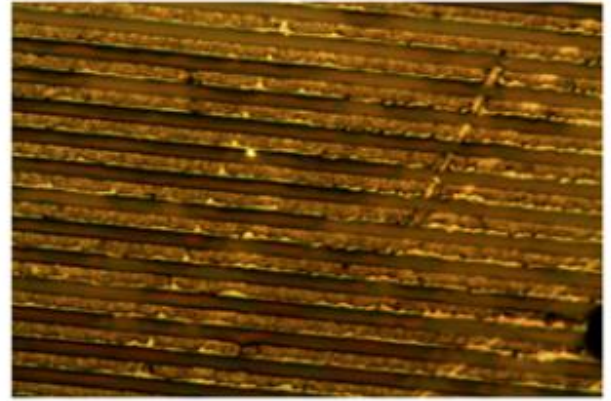


Fig. 49 Spectrum of water on the microfluidic channel network.

In Fig.49, a peak at 562 nm is formed when the water is placed on the microfluidic channel for observation. Since the water has very low absorbance in the visible region (from figure 50a), the transmittance is high in the visible region, which is observed in the spectrum.



a



b

Fig. 50 a) The water absorption spectrum over the entire electromagnetic radiation [27]; b) The microscopic image of the water on the microfluidic channel network.

From the obtained spectrum, it can be seen that the developed spectrometer works precisely. The designed spectrometer is universal, and hence, it can be adapted with any optical systems for detection.

Conclusions

1. The fluid flow rate is determined, and it is laminar for the uniform distribution of the concentration of the sample specimen. The velocities and the corresponding Reynolds number are calculated. The flow is found to be laminar at lower flow rates. The rate of flow of fluid (Q) on the microchannel is 0.25 $\mu\text{l}/\text{min}$. The fluid flow rate of 0.25 $\mu\text{l}/\text{min}$ is maintained for all the three sample specimen on the microfluidic channel network. Hence, the concentration of the sample is uniform throughout the microchannel during the experiment.
2. A visible light spectrometer is designed to be placed in the NIKON LV150 microscope. The overall dimensions of the designed spectrometer are 190mm*80mm*65mm. A step is created for the placing of the mirror on the spectrometer. Rainbow Symphony diffraction grating with 1000 lines/mm is chosen as dispersing element for the spectrometer. TRUST WEB CAMERA 16428 is chosen as detection element for the spectrometer. The spectrometer is designed for detecting light in the visible region with wavelength ranging from 380 nm to 740 nm.
3. The designed parts of the spectrometer are manufactured using 3d printing and are given black paint. A slit of 50 μm width and 6mm length is created on the top cover of the spectrometer. The mirror is placed at an angle of 45° on one end of the main assembly box to focus the beam on to the grating. The grating and the camera are placed at an angle of 30° on the other end of the main assembly box. Finally, the parts of the spectrometer are assembled.
4. The experiments are performed to test the developed visible light spectrometer. The spectrum of the three samples of water, Glycerinum and olive oil is obtained using the visible light spectrometer. Both the spectrums of water and Glycerinum show the high transmittance near the visible region. The spectrum of the olive oil denotes the presence of chlorophyll B pigment, which is responsible for the greenish colour of the olive oil. All of the above results obtained from the sample spectrum exhibits the accuracy of the designed visible light spectrometer.

References

1. D. Harvey, MODERN ANALYTICAL CHEMISTRY, The McGraw-Hill Companies, Inc.
2. C. Woodford, “Mass spectrometer,” 2018. [Online]. Available: <https://www.explainthatstuff.com/how-mass-spectrometers-work.html>.
3. E. d. Hoffmann and V. Stroobant, Mass spectrometry principles and applications, John Wiley & Sons Ltd.
4. O. Khan, “Chemistry Libre texts,” December 2018. [Online]. Available: [https://batch.libretexts.org/print/A4/url=https://chem.libretexts.org/Bookshelves/Analytical_Chemistry/Supplemental_Modules_\(Analytical_Chemistry\)/Instrumental_Analysis/Mass_Spectrometry/Mass_Spectrometers_\(Instrumentation\)/Mass_Analyzers_\(Mass_Spectromet](https://batch.libretexts.org/print/A4/url=https://chem.libretexts.org/Bookshelves/Analytical_Chemistry/Supplemental_Modules_(Analytical_Chemistry)/Instrumental_Analysis/Mass_Spectrometry/Mass_Spectrometers_(Instrumentation)/Mass_Analyzers_(Mass_Spectromet). [Accessed 29 October 2019].
5. H. Lingerman, “Chrom media analytical sciences,” How to select a technique, 2019. [Online]. Available: <http://www.chromedia.org/chromedia?waxtrapp=yooovpDsHiemBpdmBIIecCI&subNav=yarwnEsHiemBpdmBIIecCIbB>. [Accessed 4 November 2019].
6. Y. Fainman, L. P. Lee, D. Psaltis and C. Yang, Optofluidics Fundamentals, Devices and Applications, The McGraw-Hill Companies, Inc.
7. X. Fan and I. M. White, “Optofluidic Microsystems for Chemical and Biological Analysis,” *Nature photonics*, no. 5(10): 591–597.
8. L. Pang, L. Uriel, K. Campbell, A. Groisman and Y. Fainman, “Set of two orthogonal adaptive cylindrical lenses in a monolith elastomer device,” vol. OPTIC EXPRESS, no. Issue 22, pp. 9003-9013 (2005).
9. C. Barbaros, M. B. Özerb and M. E. Solmaz, “Microfluidic bio-particle manipulation for biotechnology,” vol. Biochemical engineering journal, 2014.
10. D. D and G. T, “Optical biosensors: a revolution towards quantum nanoscale electronics device fabrication,” *Journal of Biomedicine and Biotechnology*, vol. 2011, 2011.
11. Y. Guo, H. Li, K. Reddy, V. R. Nittoor and H. S. Shelar, “Optofluidic Fabry–Pérot cavity biosensor with integrated flow-through micro-/nanochannels,” *Applied physics letter*, vol. 2011.

12. G. Safina, "Application of surface plasmon resonance for the detection of carbohydrates, glycoconjugates, and measurement of the carbohydrate-specific interactions: A comparison with conventional analytical techniques. A critical review," vol. *Analytica Chimica Acta*, no. 712.
13. M. A. Cooper, "Optical biosensors in drug discovery," *Nature reviews - Drug Discovery*, t. 1, pp. 515-528.
14. J. L. Hammond, N. Bhalla and P. Estrela, "Localized Surface Plasmon Resonance as a Biosensing Platform for Developing Countries," no. 4(2) 172-188, 2014.
15. M. Benford, G. L. Coté, J. Kameoka and M. Wang, "Raman Detection," in *Handbook of Optofluidics*, New York, CRC Press, Taylor & Francis group.
16. D. Harvey, "UV/VIS AND IR SPECTROSCOPY," [Online]. Available: <https://chem.libretexts.org/link?5610>. [Accessed august 2019].
17. B. Narijauskaite, A. Palevičius, P. Narmontas, M. Ragulskis and G. Janušas, "High-Frequency Excitation for Thermal Imprint High-Frequency Excitation for Thermal Imprint," vol. *Experimental Techniques*, 2010.
18. J.-t. Teng, J.-C. Chu, C. Liu, T. Xu, Y.-F. Lien, J.-H. Cheng, S. Huang, S. Jin, T. Dang, C. Zhang, X. Yu, M.-T. Lee and R. Greif, "Fluid Dynamics in Microchannels, Fluid Dynamics, Computational Modeling and Applications".
19. Bürkle GmbH, "Viscosity of liquids," Bürkle GmbH, 2016.
20. Engineering Toolbox, "Liquid densities," [Online]. Available: https://www.engineeringtoolbox.com/liquids-densities-d_743.html. [Accessed 11 November 2019].
21. NIKON, "NIKON INDUSTRIAL MICROSCOPE ECLIPSE LV150/150A MANUAL," NIKON.

22. A. Scheeline, "How to Design a Spectrometer," Vols. Applied Spectroscopy 2017, Vol. 71(10) 2237–2252, no. <https://doi.org/10.1177/0003702817720468>, 2017.
23. Thermino system, "Thermino Spectrometer technology," Thermino system, 15 August 2014. [Online]. Available: https://www.thermino.com/wp-content/uploads/files/Thermino_Spectrometer_Technology_ENG.pdf.
24. Thorlabs, "Visible transmission gratings," Thorlabs, 2017. [Online]. Available: https://www.thorlabs.com/newgrouppage9.cfm?objectgroup_id=1123. [Accessed 14 November 2019].
25. D. C. . A. De Caro and D. M. Schubnell, "Quality control of olive oil by UV/VIS," *METTLER TOLEDO Thermal Analysis UserCom 42*.
26. N. MR, Y. Z, Q. W, P. MA and C. X, "Purification of Crude Glycerol using Acidification: Effects of Acid Types and Product Characterization," vol. Austin Chemical Engineering, no. Volume 1 Issue 1 - 2014, July 14, 2014.
27. Rohlf, "Transparency of Water in the Visible Range," [Online]. Available: <http://230nsc1.phy-astr.gsu.edu/hbase/Chemical/watabs.html>.

Appendices

Appendix 1. Manufactured parts

Main assembly box:



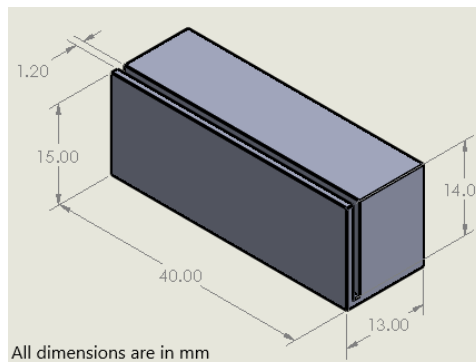
Top cover:



Side cover:



Appendix 2. Grating holder



Appendix 3. Bench test spectrum



4

3

2

1

F

F

E

E

D

D

C

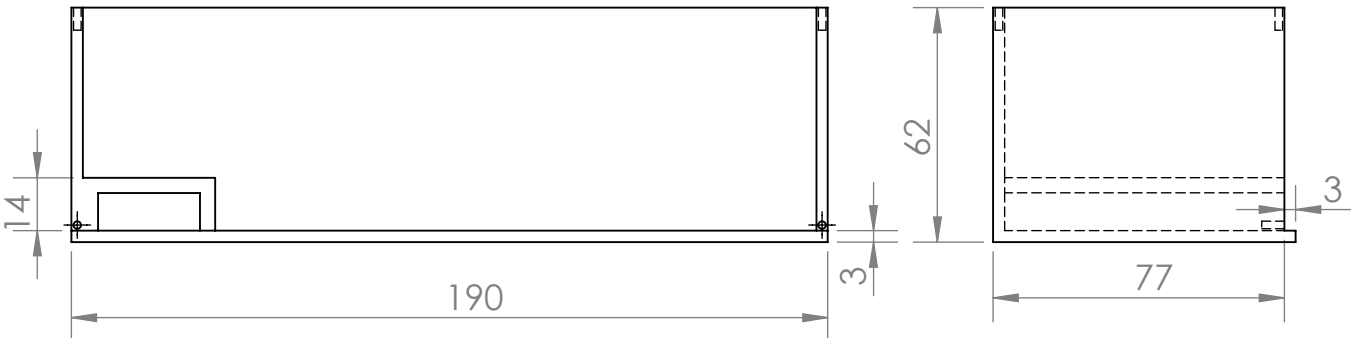
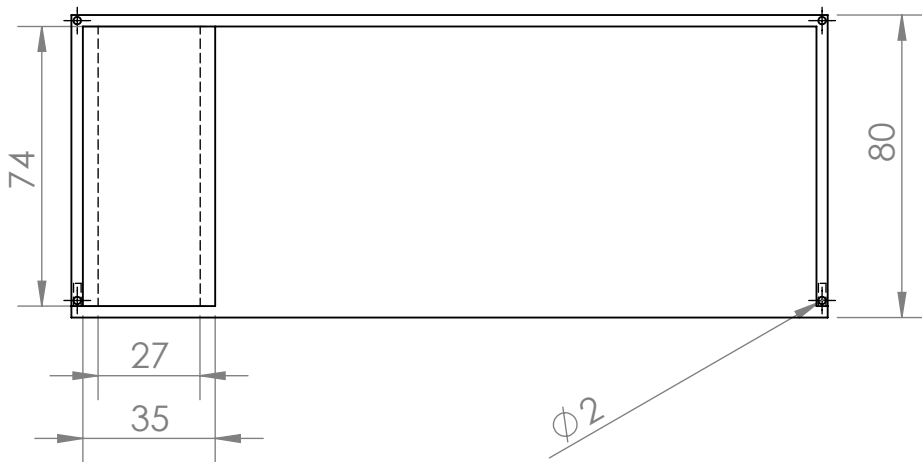
C

B

B

A

A



			REVISION	
			TITLE: Main assembly box	
NAME	DATE	MATERIAL: PLA		
DRAWN Harish Balasubramanian	24/10/19	DWG NO. 1		
CHKD Harish Balasubramanian	24/10/19	A4		
APPVD Giedrius Janušas	24/10/19	SCALE: 1:5		
MFG Harish Balasubramanian	4/11/19	SHEET 1 OF 1		
Q.A Giedrius Janušas	5/11/19			
WEIGHT:		SCALE: 1:5		SHEET 1 OF 1

4

3

2

1

4

3

2

1

F

F

E

E

D

D

C

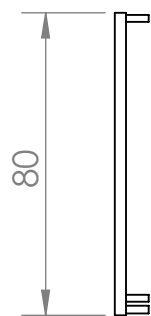
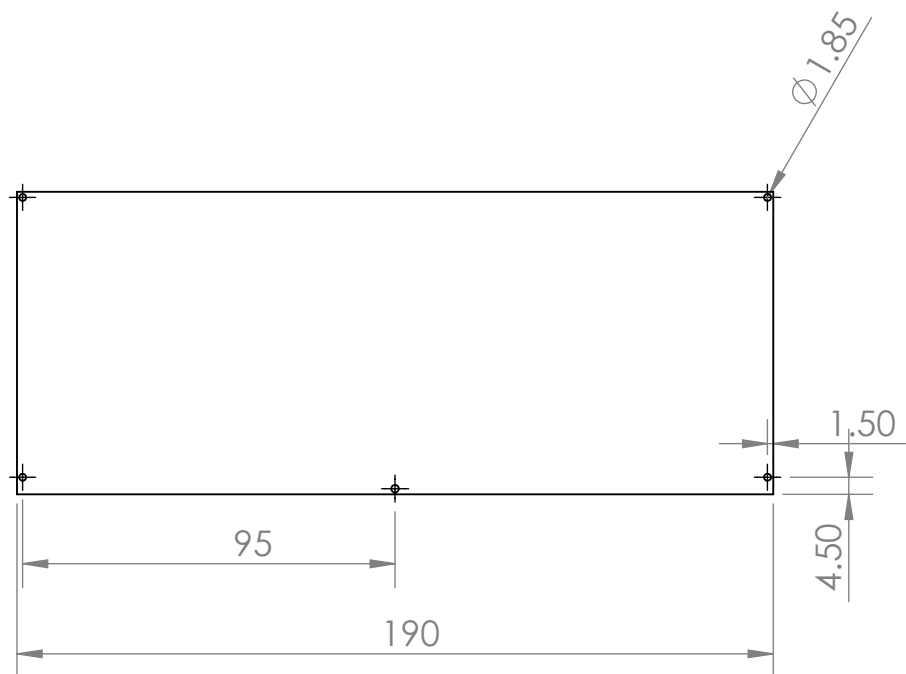
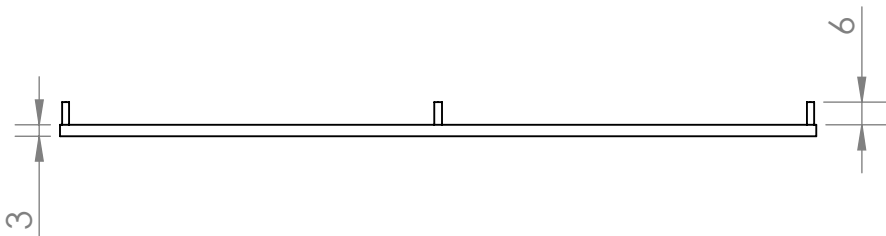
C

B

B

A

A



			REVISION	
			TITLE: Top Cover	
NAME	DATE		DWG NO. 2	
DRAWN Harish Balasubramanian	24/10/19		A4	
CHKD Harish Balasubramanian	24/10/19			
APPVD Giedrius Janušas	24/10/19			
MFG Harish Balasubramanian	4/11/19			
Q.A Giedrius Janušas	5/11/19	MATERIAL: PLA	SCALE:1:2	
		WEIGHT:	SHEET 1 OF 1	

4

3

2

1

4

3

2

1

F

F

E

E

D

D

C

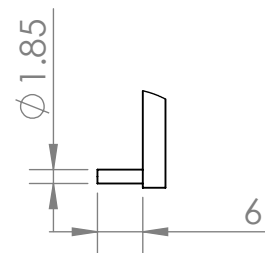
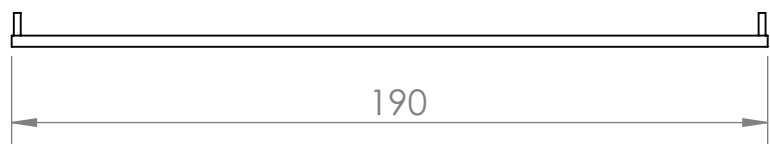
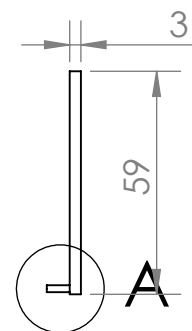
C

B

B

A

A



DETAIL A

SCALE 1 : 1

REVISION

NAME		DATE		
DRAWN	Harish Balasubramanian	24/10/19		
CHKD	Harish Balasubramanian	24/10/19		
APPVD	Giedrius Janušas	24/10/19		
MFG	Harish Balasubramanian	4/11/19		
Q.A	Giedrius Janušas	5/11/19		
			MATERIAL:	
			PLA	
			WEIGHT:	

TITLE:

Side Cover

DWG NO.

3

A4

SCALE:1:2

SHEET 1 OF 1

4

3

2

1